

# GeMS in the Outer Galaxy: Near-Infrared Imaging of Three Young Clusters at Large Galactic Radii<sup>1</sup>

T. J. Davidge

*Dominion Astrophysical Observatory,  
National Research Council of Canada, 5071 West Saanich Road,  
Victoria, BC Canada V9E 2E7*

## ABSTRACT

Images recorded with the Gemini South Adaptive Optics Imager (GSAOI) and corrected for atmospheric seeing by the Gemini Multiconjugate Adaptive Optics System (GeMS) are used to investigate the stellar contents of the young outer Galactic disk clusters Haffner 17, NGC 2401, and NGC 3105. Ages estimated from the faint end of the main sequence (MS) and the ridgeline of the pre-main sequence (PMS) on the  $(K, J - K)$  color-magnitude diagrams are consistent with published values that are based on the MS turn-off, with the GSAOI data favoring the younger end of the age range for NGC 2401 in the literature. The mass function (MF) of NGC 2401 is similar to that in the Solar neighborhood, and stars spanning a wide range of masses in this cluster have similar clustering properties on the sky. It is concluded that NGC 2401 is not evolved dynamically. In contrast, the MF of Haffner 17 differs significantly from that in the Solar neighborhood over all masses covered by these data, while the MF of NGC 3105 is deficient in objects with sub-solar masses when compared with the Solar neighborhood. Low mass objects in Haffner 17 and NGC 3105 are also more uniformly distributed on the sky than brighter, more massive, MS stars. This is consistent with both clusters having experienced significant dynamical evolution.

*Subject headings:* Open Clusters and Associations: Haffner 17, NGC 2401, NGC 3105 – Stars: luminosity function, mass function – Stars: pre-main sequence

---

<sup>1</sup>Based on observations obtained at the Gemini Observatory, which is operated by the Association of Universities for Research in Astronomy, Inc., under a cooperative agreement with the NSF on behalf of the Gemini partnership: the National Science Foundation (United States), the National Research Council (Canada), CONICYT (Chile), the Australian Research Council (Australia), Ministério da Ciência, Tecnologia e Inovação (Brazil) and Ministerio de Ciencia, Tecnología e Innovación Productiva (Argentina).

## 1. INTRODUCTION

It is generally believed that stars do not form in isolation, although the clusters and associations in which they form are subject to disruption by a combination of internal (e.g. winds and supernovae) and external (e.g. interactions with giant molecular clouds) processes. Evidence that most clusters are short-lived comes from studies of the disks of nearby galaxies, which reveal that the majority of stars belong to the so-called ‘field’ (e.g. Silva-Villa & Larsen 2011). While a few clusters in disk environments survive their first few Myr, the pace of cluster disruption continues at a rapid pace, with a destruction rate of roughly an order of magnitude per decade in age for systems older than 10 Myr (Fall & Chandar 2012).

Young star clusters at large Galactocentric radii ( $R_{GC}$ ) are of interest as they probe evolution in an environment that is systematically different from the Solar neighborhood. The relatively low density of the outer Galactic disk will affect the pace of cluster evolution that is driven by external processes, with the result that internal processes may play a larger role in the structural evolution of clusters at large  $R_{GC}$  than in the Solar neighborhood. In addition, the metallicity of young objects tends to drop with increasing  $R_{GC}$ , and a lower metallicity may allow protostars in outer disk clusters to accrete material for longer periods of time than in the solar neighborhood, thereby altering the stellar MF near what will eventually become the bottom of the MS (e.g. De Marchi et al. 2011). Finally, if galactic disks form from the inside-out then clusters that are dissolving near the periphery of the present day disk may be contributing a significant fraction of the local field star component – studies of such clusters might then yield insights into the assembly of the field star population at large  $R_{GC}$ .

In the present paper, images corrected for atmospheric distortions by the Gemini South Muti-conjugate Adaptive Optics System (GeMS) and recorded with the Gemini South Adaptive Optics Imager (GSAOI) are used to probe the near-infrared photometric properties and

spatial distributions of MS stars and PMS objects in three young clusters in the outer Galaxy: Haffner 17, NGC 2401, and NGC 3105. These clusters were selected for this program based on their (1) location outside of the Solar Circle, (2) age ( $\leq 0.1$  Gyr), (3) distance ( $\geq$  a few kpc), and (4) angular size ( $r \leq 1.5$  arcmin). Near-infrared observations of these clusters are of interest since they are at low Galactic latitude, and so they may be subject to significant amounts of extinction. The high angular resolution delivered by GeMS is useful for overcoming the crowding that might be an issue at faint magnitudes while also allowing wide binary systems to be resolved. The latter are of interest as the binary frequency in a cluster provides insights into its dynamical state and the population of isolated low mass objects that will ultimately find their way into the field (e.g. Marks & Kroupa 2011).

The ages, distance moduli ( $\mu_0$ ), and reddenings of the clusters, taken from the August 2013 version of the WEBDA (Mermilliod 1995) database, are listed in Table 1. Also listed are  $K$  magnitudes and radii obtained from 2MASS images. The magnitudes and radii are total values estimated from growth curves, and the integrated magnitudes of all three clusters are subject to significant sources of uncertainty. NGC 2401 is a diffuse cluster, and its total brightness is susceptible to subtle variations in the sky background in the 2MASS images. As for Haffner 17 and NGC 3105, the integrated brightnesses of both clusters are affected by bright stars near the cluster centers. In the case of NGC 3105 the total  $K$  magnitude drops by 2.1 magnitudes if the light from the two brightest stars is excluded.

In the only published photometric study of Haffner 17, Pedredos (2000) used  $UBV$  CCD measurements to find  $E(B - V) = 1.26 \pm 0.04$ ,  $\mu_0 = 12.3 \pm 0.2$ , and an age of 50 Myr. Comparisons with isochrones lead Pedredos (2000) to suggest that Haffner 17 may have a super-solar metallicity, although this is based on two red stars that may or may not be cluster members. If this metallicity is verified spectroscopically then Haffner 17 would be a rare example of a young metal-rich cluster at large  $R_{GC}$ .

NGC 2401 has been the subject of three recent studies that have yielded a range of

ages. Sujatha et al. (2004) present a CMD that shows a well-defined MS turn-off (MSTO) and numerous candidate evolved stars. They find an age of 0.1 Gyr, a distance of 3.5 kpc, and  $E(B - V) = 0$ . In contrast, Baume et al. (2006) measure an age of 25 Myr, a distance of  $6.3 \pm 0.5$  kpc, and  $E(B - V) = 0.36$ . Significantly, Baume et al. (2006) also detect a population of possible PMS objects with  $V \geq 17 - 18$ , and a Be star that may be a cluster member – both of these findings are consistent with a younger age than found by Sujatha et al. (2004). Most recently, Hasegawa et al. (2008) find a distance of 5.6 kpc for NGC 2401, with an age of 0.1 Gyr and  $E(V - I) = 0.3$ , which corresponds to  $E(B - V) \sim 0.24$ . A curious aspect of the Hasegawa et al. (2008) study is that the isochrones in their Figure 2 do not match the CMD near the MSTO, in the sense that there are blue stars with MS-like colors that form a well-defined sequence above the MSTO of the 100 Myr isochrone. If these blue stars are actual members of NGC 2401 and define the MSTO, as opposed to blue stragglers or field stars with fortuitous photometric properties, then the age estimated for NGC 2401 by Hasegawa et al. (2008) is too old.

NGC 3105 has one of the largest  $R_{GC}$  of any young cluster yet discovered in the Galactic disk. Early studies by Moffat & Pim Fitzgerald (1974) and Pim Fitzgerald et al. (1977) found evidence of numerous Be stars and supergiants, pointing to a young age. Sagar et al. (2001) measured  $E(B - V) = 1.06$ , a distance of  $9.5 \pm 1.5$  Mpc, and an age of  $25 \pm 10$  Myr. More recently, Paunzen et al. (2005) found  $E(B - V) = 0.95 \pm 0.02$ , a distance of  $8.53 \pm 1.03$  kpc, and an age  $\log(t) = 7.30 \pm 0.1$  (i.e.  $t = 20_{-4}^{+5}$  Myr).

The data discussed here are used to examine the  $(K, J - K)$  CMDs of the clusters, with specific emphasis on the magnitude interval that contains PMS objects and the lower reaches of the MS. The ages of young clusters can be estimated using the brightness of the MS cut-off (MSCO) and the position of the PMS sequence on the CMD. Assuming a standard MF then this part of the CMD is less susceptible to the stochastic effects that can affect the properties of the more massive cluster members that define the MSTO. Insights

can also be gleaned into the dynamical state of the clusters and – possibly – their early evolution by examining the  $K$  luminosity function (LF) and spatial distributions on the sky of their component stars.

The observations are summarized in Section 2, while the reduction of the data and the techniques used to make the photometric measurements are discussed in Section 3. The CMDs are presented and examined in Section 4, while the LFs and spatial distributions of stars within the clusters are the subjects of Sections 5 and 6. The paper closes in Section 7 with a discussion and summary of the results.

## 2. OBSERVATIONS

The data were recorded in January and February 2013 as part of program GS-2012B-SV-409. Details of the observations are summarized in Table 2. This program utilized two new Gemini capabilities – the GeMS adaptive optics system and the GSAOI – and these are briefly described below.

GeMS (Rigaut et al. 2012; Neichel et al. 2012) is the facility adaptive optics (AO) system on Gemini South. GeMS monitors wavefront distortions using information provided by five laser guide stars, up to three natural guide stars (NGSs), and an on-detector guide source. The result is a seeing-corrected signal that covers a much larger angular area on the sky than is delivered by – say – a single beacon AO system that is conjugated to the telescope primary mirror.

The brightnesses and locations of the NGSs in the GeMS field play a key role in determining the degree of correction and the angular stability of the point spread function (PSF). In sparse stellar environments the choice of NGSs may be problematic, with selection based on the few available objects that are bright enough to serve as NGSs. Fortunately, the rich population of bright cluster members and field stars provided a number of potential

NGSs for the present program. Three NGSs that defined a more-or-less equilateral triangle-shaped asterism were identified for each cluster, and **the mean  $R$  magnitudes of these,  $\langle R \rangle$ , are listed in Table 2.** While the degree of correction and the stability of the PSF across the field depends on a number of factors, such as guide star brightness and the atmospheric conditions in the dominant turbulent layers, an equilateral triangle-shaped asterism should deliver a near-optimum level of PSF uniformity across the GSAOI field.

The wavefront-corrected beam from GeMS was imaged by GSAOI (McGregor et al. 2004; Carrasco et al. 2012), which was designed specifically for use with GeMS. The detector in GSAOI is a mosaic of four  $2048 \times 2048$  HgCdTe arrays that cover an  $85 \times 85$  arcsec area with  $0.02 \text{ arcsec pixel}^{-1}$  sampling. Gaps between the arrays form a cross-shaped pattern with 3 arcsec wide arms on the sky.

Images were recorded through  $J$ ,  $Ks$ , and  $\text{Br}\gamma$  filters, with short and long exposure times to allow a wider magnitude range to be sampled than is possible with only a single exposure time. A three point (short exposure) and five point (long exposure) linear north/south dither pattern was employed that allowed one arm of the gap on the detector mosaic to be filled. **The cluster fields are not crowded, and so the seeing requirements for this program were set to 85%ile. The Fried (1966) parameter,  $r_0$ , provides one measure of image quality. The  $r_0$  measurement taken from the image header of the exposure that was recorded midway through the observing sequence for each cluster is listed in Table 2. The seeing degrades as  $r_0$  moves to smaller values. During a seeing campaign in 1998, Vernin et al. (2000) found a mean  $r_0$  of 19 cm on Cerro Pachon, with a minimum  $r_0$  of 5 cm, and a maximum of 40 cm. The values of  $r_0$  listed in Table 2 are less than the mean found by Vernin et al. (2000), indicating that these measurements were made during worse than normal seeing conditions, as was intended.**

The mean FWHM values,  $\langle FWHM \rangle$ , and the standard deviation about these

means,  $\sigma_{FWHM}$ , are also listed in Table 2. These gauge the level of correction and the uniformity of the PSF across the GSAOI field, and the entries in Table 2 were measured from the PSF stars that were used in the photometric analysis of the long exposure images (Section 3). The PSF stars in the Br $\gamma$  images have similar FWHMs to those in  $Ks$ , and so  $\langle FWHM \rangle$  and  $\sigma_{FWHM}$  are not listed for that filter.

The angular resolution delivered by an AO system during given seeing conditions depends on wavelength, in the sense that as one moves to longer wavelengths then the corrected angular resolution will approach the telescope diffraction limit at that wavelength. At the same time, the PSF will also become more uniform across the field (i.e.  $\sigma_{FWHM}$  in Table 2 should decrease). The entries in Table 2 show that both the angular resolution and stability of the FWHM across the field is better in  $Ks$  than in  $J$ , as expected.

**The telescope diffraction limit,  $1.2 \times \frac{\lambda}{D}$ , where  $D$  is the diameter of the primary mirror, is 0.04 arcsec in  $J$ , and 0.07 arcsec in  $Ks$ . The  $Ks$  images of NGC 2401 have angular resolutions that come closest to the system diffraction limit. The entries in Table 2 indicate that GeMS can deliver  $\sim 0.1$  arcsec angular resolution images in  $J$  and  $Ks$  with a stability in the FWHM of 10% across the GSAOI field even when the imaging conditions are less than ideal.**

### 3. DATA REDUCTION & PHOTOMETRY

#### 3.1. Producing Final Images

The initial processing of the data followed standard procedures for near-infrared imaging. The basic steps were (1) dark subtracton, (2) flat-fielding, and (3) the removal of thermal emission artifacts that are produced by warm objects along the optical path, such as dust on the GSAOI entrance window. The first two steps used calibration frames that were recorded specifically for these purposes. As for the third step, calibration frames were constructed by

median-combining the flat-fielded long exposure images of all program clusters on a filter-by-filter basis after these were processed to correct for differences in exposure time and sky level (see below). The resulting calibration frames are not ‘sky flats’, as they are constructed from images that have already been corrected for flat-field variations. Rather, they monitor an additive component in the background that constitutes a significant source of noise.

To construct the background calibration frames it is necessary to create a homogeneous set of images that have a common effective exposure time and have been corrected for variations in the background sky level, which can be significant over timescales of a few minutes in the near-infrared. The individual cluster images were first normalized to a common exposure time (1 second in this case). A constant sky level, measured by taking the mode of pixel intensities in each frame, was then subtracted from each image. As four different clusters were observed and the data were recorded with on-sky dithering, then the median intensity of all images at each GSAOI detector pixel is expected to be free of contamination from bright and moderately bright sources, leaving only thermal emission signatures. This expectation was borne out by visual inspection of the background calibration frames.

The penultimate processing step is to correct for distortions that are introduced by the GeMS and GSAOI optics, and are manifest as a change in pixel scale with location in the images. These distortions are primarily (but not exclusively) radial in nature and are most obvious near the edge of the science field in images that are registered near the center of the GSAOI field. They can appear either as filter-dependent differences in source centroids or as differences between source centroids in images recorded in the same filter but at different points in the on-sky dither pattern.

When comparing observations recorded in different filters, the offsets are largest when  $J$  and  $Ks$  images are compared, where they can amount to differences in image centroids of a tenth of an arcsec (i.e. a few GSAOI pixels) near the edge of the GSAOI science field. Offsets of a few hundredths of an arcsec (i.e. a GSAOI pixel) are typical when  $Br\gamma$  and



$K_s$  images are compared. To obtain a common reference grid for image combination and photometric analysis, the  $J$ ,  $Br\gamma$ , and dithered  $K_s$  images were geometrically transformed using the IRAF Geomap and Geotran tasks into the reference frame defined by the  $K_s$  image recorded at the null position of the dither pattern. The final images for each cluster were then found by taking the median signal level on a filter-by-filter basis at each pixel location in the transformed and aligned images.

### 3.2. Photometric Measurements, Calibration, and Characterization

Stellar brightnesses were measured with the PSF-fitting program ALLSTAR (Harris & Stetson 1988). PSFs for each cluster were constructed from between 15 to 20 stars using the *PSF* routine in the DAOPHOT (Stetson 1987) package. The same stars were used to construct the PSFs in all three filters. The wings of AO-corrected PSFs typically extend out to radii that are comparable to the uncorrected seeing disk, and a 1 arcsec PSF extraction radius was used here.

PSF stars were selected based on brightness and the absence of obvious companions. An additional criterion was location in the GSAOI science field, with the intent of obtaining a more-or-less uniform distribution of PSF stars across the  $85 \times 85$  arcsec<sup>2</sup> field. Monitoring the PSF at various points across the science field is important as modest residual PSF variations remain in the GeMS-corrected beam. The  $\sigma_{FWHM}$  entries in Table 2 indicate that there are variations in the FWHM of PSF stars of up to a few hundredths of an arcsec, and a visual inspection of the FWHM values over the GSAOI field indicated that modest systematic trends were evident. In fact, photometry obtained with a PSF that has a first order spatial variation delivered tighter sequences on the CMDs than those that resulted from the application of a constant PSF. Still, the differences between the CMDs that result from the application of fixed and variable PSFs are not large, and the basic results of this study would not change substantially if fixed PSFs were used to obtain the photometry.

The  $J$  and  $K_s$  photometry was calibrated using 28 observations of 13 Persson et al. (1998) standard stars that were recorded throughout the GeMS SV run. The  $1\sigma$  formal error in the  $J$  and  $K$  zeropoints is  $\pm 0.04$  magnitude, with a standard deviation about the mean of  $\pm 0.13$  magnitudes. The calibration was checked against photometric measurements made from 2MASS images, although the vastly different angular resolutions and faint limits of the GSAOI and 2MASS observations limits the number of suitable stars that can be used in such a comparison. The GSAOI and 2MASS images were also recorded at different epochs, and so stellar variability is a potential source of scatter. The brightnesses of sources in the 2MASS images of the clusters were measured with ALLSTAR, and the results were calibrated using relevant information in the 2MASS image headers. Restricting the comparisons to isolated objects with  $K < 14.5$ , then the mean differences between the two datasets are  $\Delta(K) = 0.06 \pm 0.05$  and  $\Delta(J - K) = -0.08 \pm 0.09$ . These differences are in the sense GSAOI–2MASS, and the quoted uncertainties are  $1\sigma$  errors in the mean. It is evident that the GSAOI and 2MASS measurements are in a consistent photometric system. A similar conclusion was reached by Davidge et al. (2013), based on comparisons of GSAOI and 2MASS ( $K, J - K$ ) CMDs of the cluster Haffner 16, which was also observed as part of program GS-2012B-SV-409.

The calibration of the  $Br\gamma$  images is tied to the  $K_s$  calibration. The central wavelengths and the mean throughputs of the  $Br\gamma$  and  $K_s$  filters are not vastly different, and a zeropoint for the  $Br\gamma$  filter was found by scaling the  $K_s$  zeropoint to compensate for the difference in the effective bandpasses between the two filters. As shown in the next section, this scaling results in  $Br\gamma - K_s \sim 0$  for most sources.

Artificial star experiments were run to determine sample completeness and to characterize uncertainties in the photometry. The artificial stars were con-

structed by scaling the PSFs that were used to make the photometric measurements and were assigned  $J - K$  and  $Br\gamma - K$  colors that are representative of the cluster sequences on the CMDs. As with real stars, an artificial star was considered to be recovered only if it was detected in two filters (either  $J + K$  or  $Br\gamma + K$ ). The artificial star experiments indicate that the completeness fractions near the faint end of the CMDs vary from cluster-to-cluster, as expected due to differences in angular resolution. The  $(K, J - K)$  CMDs of all three clusters are complete when  $K \leq 19.5$ .

## 4. COLOR-MAGNITUDE DIAGRAMS

### 4.1. A First Look at the $(K, J - K)$ CMDs

The  $(K, J - K)$  CMDs of the clusters are presented in Figures 1 – 3. The blue error bars in the left hand panels show the  $\pm 1\sigma$  random uncertainties in  $J - K$  computed from the artificial star experiments. The predicted dispersion more-or-less matches the observations at  $K = 19$  and  $K = 20$ , suggesting that the scatter at the faint end of the CMDs is dominated by photometric errors. In contrast, at  $K \leq 18$  the random uncertainties tend to be narrower than the observed scatter, suggesting that the width of the CMDs at these magnitudes reflects an intrinsic dispersion in the photometric properties of objects.

The CMD of Haffner 17 has a moderately tight sequence with  $K < 18$  that is dominated by cluster stars. The scatter that is present at most magnitudes is likely due to a mix of cluster members, which are a combination of main sequence and PMS objects, and field stars. Star counts from the Robin et al. (2003) model suggest that the fraction of field stars in the Haffner 17 CMD ranges from 30% at the bright end to 70% at the faint end. These numbers were computed using the full range of stellar types available for the Robin

et al. (2003) model, with the reddening assumed to be uniformly distributed along the line of sight towards the cluster. These assumptions are used for all star count models discussed throughout this work.

The dominant sequence of objects on the NGC 2401 CMD is not as well-defined as in the other two clusters. Baume et al. (2006) present a near-infrared CMD of NGC 2401 obtained from 2MASS images that also shows substantial scatter. The dispersion along the color axis is likely not due to differential reddening. If this were the case then  $\Delta E(B - V) \sim 0.4 - 0.6$  magnitudes across the GSAOI field. Differential reddening of this size would be surprising given that stars in NGC 2401 have an average  $E(B - V) = 0.15$  (Section 4.2). There are also no obvious dust lanes in the DSS or 2MASS images of NGC 2401. The star count models of Robin et al. (2003) suggest that 25 – 30% of the objects in the CMD of NGC 2401 are field stars, and we suspect that contamination from these objects is the dominant source of the scatter along the  $J - K$  axis.

NGC 3501 has the most richly populated CMD in our sample. A locus of cluster stars can be seen, although there is substantial scatter. Comparisons with star count models from Robin et al. (2003) suggest that field stars account for 40% of objects near the bright end of the NGC 3105 CMD and 60% of the objects near the faint end. Hence, much of the scatter is due to field stars. Of particular interest for the current work is the sequence of objects with  $J - K \sim 1$  that runs from  $K = 17.5$  to  $K = 19$ . Comparisons with isochrones indicate that this sequence is populated by PMS objects that belong to NGC 3105 (Section 4.2).

## 4.2. Comparisons with Isochrones

The CMDs are compared with Padova Isochrones in the middle and right hand panels of Figures 1 – 3. These isochrones, which are described by Bressan et al. (2012), are of interest for the present work as they include PMS evolution. The isochrones used here have

a metallicity  $Z = 0.016$ , which provides a consistent point of comparison with previous studies. The consequences of adopting different metallicities on the distance, reddening, and age estimates are examined in the next section.

The comparisons in the middle panels of Figures 1 – 3 use reddenings and distance moduli from Pedredos (2000) for Haffner 17, Baume et al. (2006) for NGC 2401, and Paunzen et al. (2005) for NGC 3501.  $E(J - K)$  was computed from the published  $E(B - V)$  values using the relations in Table 6 of Schlegel et al. (1998). It can be seen from the middle panels of Figures 1 – 3 that the published reddenings and distance moduli can be adjusted to achieve better agreement between the isochrones and the observations. To this end, independent reddenings, distances, and ages were found by comparing the properties of MS and PMS stars in the clusters with the isochrones. These revised parameters, which were used to make the comparisons in the right hand panels of Figures 1 – 3, are discussed in the following sections.

#### 4.2.1. *Reddenings and Distance Moduli*

$E(J - K)$  was found by matching the models to the blue edge of the near-vertical upper MS segment on the CMDs. There is also a vertical plume of faint red objects that is most clearly defined in the NGC 2401 CMD in Figure 2, which is another potential probe of reddening. However, the isochrones indicate that this feature is populated by a mix of field and cluster stars, and so gives only a loose check on cluster reddening.

In order to make comparisons with published reddenings,  $E(B - V)$  was calculated from  $E(J - K)$  using the reddening relations listed in Table 6 of Schlegel et al. (1998). Random uncertainties were estimated by perturbing the adopted reddening and determining the smallest change in this quantity that noticeably degraded the agreement between the isochrones and the observations. These experiments suggest that the random uncertainties

are  $\pm 0.02$  magnitudes in  $E(J - K)$ , and  $\pm 0.03$  magnitudes in  $E(B - V)$ . Departures from the reddening law used here are an obvious source of systematic uncertainty in the  $E(B - V)$  values.

The CMDs of systems with ages older than  $\sim 20$  Myr have a pronounced bend on the MS near  $M_K = 2$ . This feature, which is due to a change in opacity in stellar atmospheres, is employed here to determine distance. As with the reddenings, random uncertainties in the distance modulus were found by perturbing this quantity and assessing the impact on the agreement between the isochrones and the observations. These experiments suggest that the random uncertainty in the observed distance modulus is  $\pm 0.05$  magnitudes. With the reddening and distance set then an age can be estimated using the point on the CMD where the dominant stellar sequence departs from the MS as defined by old stellar systems and – for NGC 2401 and NGC 3105 – from a direct comparison between the PMS sequence and isochrones. Ages are estimated in Section 4.2.2.

The reddenings and distance moduli obtained from the GSAOI images do not show systematic effects. The reddening estimated by Predredos (2000) for Haffner 17 must be reduced to match the  $(K, J - K)$  CMD, while  $\mu_0$  must be increased. In contrast, for NGC 2401 a higher  $E(B - V)$  and a lower  $\mu_0$  are required to get good agreement with the models. Finally, for NGC 3105 the near-infrared CMD calls for both a lower  $E(B - V)$  and a lower  $\mu_0$ .

There is a metallicity gradient among young objects in the Galactic disk, and the clusters discussed here may have a sub-solar metallicity given their  $R_{GC}$ . Balser et al. (2011) find an azimuthally-averaged radial O/H gradient of  $-0.045$  dex  $\text{kpc}^{-1}$  in the Galactic disk, and NGC 3105 would then have  $[\text{O}/\text{H}] = -0.3$  dex if its metallicity follows this general trend. Still, in the absence of spectroscopic data, efforts to estimate metallicity based only on location in the Galaxy are frustrated by the variation in metallicity at a fixed  $R_{GC}$ , which is compounded by variations tied to the Galactic position angle (e.g. Balser et al. 2011). If

the range in gradients found in the Balser et al. (2011) study are adopted as representative of the entire disk then  $[O/H]$  for NGC 3105 would fall between  $-0.2$  and  $-0.5$  dex.

To assess the result of adopting different metallicities on the cluster parameters estimated from the GSAOI data, the  $(K, J - K)$  CMD of NGC 3105 is compared with non-solar metallicity isochrones in Figure 4. NGC 3105 was selected for this comparison because it has the largest  $R_{GC}$ , making it the cluster most likely to have a non-solar metallicity. Comparisons are made with  $Z = 0.010$  and  $0.025$  models, which is the range in metallicity that more-or-less reflects the  $\pm 0.2$  dex scatter that is seen in the metallicity *vs*  $R_{GC}$  curve defined by Galactic HII regions (e.g. Balser et al. 2011).

The comparisons in Figure 4 indicate that  $E(B - V)$  is not sensitive to isochrone metallicity. This is not surprising given that the reddening is determined from bright MS stars with photospheres in which energy transport is via radiative processes and electron scattering is the primary source of opacity. On the other hand, the  $Z=0.010$  and  $Z=0.025$  isochrones give  $\mu_0$  values that differ by 0.3 dex, which corresponds to 1 kpc at the approximate distance of NGC 3105. This reflects the metallicity sensitivity of stellar structure near the  $M_K = 2$  CMD feature.

#### 4.2.2. Ages

The luminosity of the MSTO is the classical benchmark for age estimates. However, the upper part of the MS may be poorly populated in young, low mass clusters. Statistical fluctuations amongst the most massive stars in low mass clusters may even introduce a systematic bias in age estimates, in the sense that ages may be overestimated on average. In contrast, the MSCO and PMS sequences are in parts of the CMD that – barring an anomalous MF – are more richly populated than the upper portions of the MS. The MSCO and PMS thus provide a means of gauging the ages of young and intermediate-age low mass

clusters that is less susceptible to statistical fluctuations in stellar content than the MSTO.

Figure 5 shows the portions of the  $(K, J - K)$  CMDs that cover the faintest MS stars and brightest PMS objects. The yellow line is a 1 Gyr isochrone that is included to show a reference ‘old’ MS. Ages are estimated using two criteria: (1) the magnitude at which the majority of stars at the blue edge of the data envelope depart from the 1 Gyr isochrone (i.e. the MSCO), and (2) direct comparisons between the isochrones and PMS sequences. It should be recalled that the age estimates made from PMS sequences are not sensitive to  $\pm 0.2$  dex changes in metallicity (Figure 4).

The modest number of sources in Haffner 17, coupled with the sizeable contamination from field stars, complicates efforts to estimate its age. The upper and lower limits of the MSCO in this cluster are indicated in the left hand panel of Figure 5. The faint limit of the MSCO is the point below which sources no longer fall within  $\pm 0.1$  magnitude of the 1 Gyr MS along the  $J - K$  axis, and is defined by the 5 points between  $K = 17.5$  and  $17.65$  that lie close to the 1 Gyr MS. **This  $\pm 0.1$  magnitude criterion in  $J - K$  exceeds the estimated random uncertainties in the photometry, and so provides a conservative means of assessing when stars are not on the MS.** Looking at brighter magnitudes, there is a  $\sim 0.2$  magnitude gap between this clump of points and the next group of points that fall close to the MS, and these define the bright limit of the MSCO estimate. Objects that scatter closely about the MS are relatively common at brighter magnitudes.

A well-defined PMS sequence is not evident in the CMD of Haffner 17, and this is likely a consequence of the flat LF of this cluster (Section 5) combined with the high levels of field star contamination. Therefore, the age estimate for this cluster is restricted to the MSCO, which suggests that Haffner 17 has an age in the range 45 – 60 Myr. This age is consistent with that estimated by Prededos (2000) from the MSTO.

Given the comparatively low level of field star contamination towards NGC 2401, the



majority of points in the middle panel of Figure 5 likely belong to that cluster. The faint limit of the MSCO for NGC 2401 is based on the clump of four points near  $K = 17$  that fall immediately to the right of the 1 Gyr MS. The next faintest clump of points that are close to the 1 Gyr MS are seen near  $K = 17.9$ , and this large gap indicates that  $K = 17$  is a reasonable estimate of the faint limit of the MSCO, **even after considering the random dispersion in  $J - K$  estimated from the artificial star experiments**. Between  $K = 17$  and 17.2 there are two points that fall within a few hundredths of a magnitude in  $J - K$  of the MS. The faintest of these at  $K = 17.2$  defines the bright limit of the MSCO for this cluster.

The age of NGC 2401 can also be estimated from PMS stars that populate the sequence of points between  $K = 17$  and 18 and scatter about the 20 Myr isochrone. Given the modest level of field star contamination then the majority of these objects are likely members of NGC 2401. Considering the MSCO and PMS ages of NGC 2401 together, then the cluster has an age in the range 20 – 30 Myr. This is consistent with the age found by Baume et al. (2006), but is much younger than the ages found by Sujatha et al. (2004) and Hasegawa et al. (2008). Assuming a normal MF – an assumption that is justified in Section 5 – then the older ages predicted by the latter two studies can not explain the absence of MS stars between  $K = 17$  and  $K = 17.9$  and the presence of objects as bright as  $K = 17$  with PMS-like photometric properties.

Field star contamination is an issue for determining the MSCO magnitude in NGC 3105. Still, there are large numbers of points that fall along – or immediately to the right of – the 1 Gyr MS isochrone to as faint as  $K = 17.7$ . Data points clustering about the MS are present at fainter magnitudes, but they form a more diffuse sequence than at brighter magnitudes **with a dispersion that exceeds that expected from random photometric errors alone**. This suggests that these objects are field stars. Therefore,  $K = 17.7$  is adopted as the MSCO faint limit in NGC 3105. Keeping with the spirit of the procedure

applied for Haffner 17 and NGC 2401, then the bright limit of the MSCO in NGC 3105 is assigned to the next brightest clump of points, which occur at  $K = 17.5$ . The age of NGC 3105 determined from the MSCO is then 25 Myr.

An age for NGC 3105 can also be estimated from PMS stars that form a locus of points in the CMD with  $K \geq 17.5$ . The majority of points on this sequence fall between the 20 and 40 Myr isochrones and are indicative of an age near  $\sim 25$  Myr, which is consistent with the age deduced from the MSCO. The age of NGC 3105 based on the MSCO and PMS is then  $\sim 25$  Myr. This agrees with the ages found by Sagar et al. (2001) and Paunzen et al. (2006).

### 4.3. $\text{Br}\gamma$ Emission

Young PMS stars that are accreting material may show Hydrogen emission lines in their spectra. The strength of this emission depends on the rate of accretion, which can vary with time. The overall accretion rate also depends on metallicity and age, in the sense that the mean accretion rate drops towards higher metallicities and older ages. Line emission is seen among PMS stars in the SMC with ages  $\sim 20 - 30$  Myr (e.g. Figure 9 of De Marchi et al. 2011). Given that (1) the clusters discussed here are in the outer regions of the Galaxy, where there is a reasonable chance that they might have a sub-solar metallicity, and (2) there is evidence that NGC 2401 and NGC 3105 have ages of 20 – 30 Myr, then it was decided to search for signatures of  $\text{Br}\gamma$  emission from bright PMS stars.

$\text{Br}\gamma$  emission lines in the spectra of very young PMS objects in the solar neighborhood have equivalent widths  $\leq 10\text{\AA}$  (e.g. Donehew & Brittain 2011). To detect similar emission lines in individual objects in the narrow-band  $\text{Br}\gamma$  filter would require photometry that is reliable to within a few hundredths of a magnitude, and this is at the limits of the photometric uncertainties of even the brightest stars in the GSAOI images. However, the mean  $\text{Br}\gamma - K$

colors of an ensemble of objects may be skewed systematically if  $\text{Br}\gamma$  emission is present in a large number of its members. Davidge et al. (2013) investigate the mean  $\text{Br}\gamma$ - $K$  colors of objects in the 10 Myr cluster Haffner 16, and find evidence of weak systematic  $\text{Br}\gamma$  emission among PMS objects in that cluster.

The  $(K, \text{Br}\gamma - K)$  CMDs of the clusters are shown in Figure 6, where the  $\pm 1\sigma$  random errors in  $\text{Br}\gamma - K$ , calculated from the artificial star experiments, and the magnitude of the MSCO are indicated. The predicted random errors in  $\text{Br}\gamma - K$  match the observed scatter near the faint ends of the CMDs. However, at intermediate magnitudes the observed scatter exceeds the predicted random errors, indicating that star-to-star differences in  $\text{Br}\gamma - K$  are present.

Sources with  $\text{Br}\gamma$  in emission lie to the left of non-emitting sources on the  $(K, \text{Br}\gamma - K)$  CMDs. The  $\text{Br}\gamma - K$  color of Haffner 17 stays roughly constant with  $K$  magnitude, with no obvious change in  $\text{Br}\gamma - K$  near the MSCO. This suggests that  $\text{Br}\gamma$  emission with equivalent widths of a few  $\text{\AA}$  is not present among the majority of PMS stars in Haffner 17.

The situation is different for NGC 2401. In the magnitude interval  $K = 14.5 - 16.3$  the majority of objects fall to the right of the  $\text{Br}\gamma - K = 0$  line, whereas between  $K = 16.3$  and 18 the majority of points fall to the left of this line. The artificial star experiments indicate that the data are complete in this magnitude range, and that the break is not due to a systematic error in the photometry. A Kolmogorov-Smirnov test indicates that the  $\text{Br}\gamma - K$  distributions in the interval  $K = 15.0 - 16.0$  differs from that in the interval  $K = 16.5 - 17.5$  at roughly the 95% confidence level. Thus, the  $\text{Br}\gamma - K$  distribution changes within  $\sim 0.6$  magnitude of the MSCO in NGC 2401.

The morphology of the  $(K, \text{Br}\gamma - K)$  CMD of NGC 3105 is similar to that of NGC 2401, but shifted  $\sim 0.6 - 0.7$  magnitudes fainter in  $K$ . A jog can be seen near  $K = 17$  in the NGC 3105  $(K, \text{Br}\gamma - K)$  CMD, in the sense that at magnitudes between  $K = 16$  and

17 the majority of points fall to the right of the  $\text{Br}\gamma - K = 0$  line, whereas between  $K = 17$  and 18 the majority of points fall to the left of this line. This break occurs at a magnitude where the data are 100% complete. A Kolmogorov-Smirnov test indicates that the  $\text{Br}\gamma - K$  distributions of sources in the intervals  $K = 16 - 17$  and  $K = 17 - 18$  differ at roughly the 97% confidence level. Therefore, as in NGC 2401, a change in the  $\text{Br}\gamma - K$  colors of sources occurs  $\sim 0.6$  magnitudes brighter than the MSCO.

The breaks in the  $(K, \text{Br}\gamma - K)$  CMDs of NGC 2401 and NGC 3105 occur near  $M_K \sim 2.5 - 2.6$ . Given that these clusters have similar ages, then that their  $(K, \text{Br}\gamma - K)$  CMDs show a feature at roughly the same  $M_K$  suggests that a common mechanism may be responsible for this change. This being said, it is not clear if the change in the  $\text{Br}\gamma - K$  distribution is due to the onset of  $\text{Br}\gamma$  emission, or to a decrease in the strength of  $\text{Br}\gamma$  absorption. PMS objects have lower surface gravities than MS stars with the same color, and so may have weaker  $\text{Br}\gamma$  absorption line strengths. The differences in the  $\text{Br}\gamma$  properties of PMS and non-PMS sequence stars in NGC 2401 and NGC 3105 could be due to such a surface gravity effect. If this is the case then the  $\text{Br}\gamma$  observations have picked up on a signature of PMS stars, albeit one that is due to a mechanism other than Hydrogen line emission.

Could the break in the  $(K, \text{Br}\gamma - K)$  CMDs not be related to PMS stars? The  $M_K$  at which the change in  $\text{Br}\gamma - K$  occurs corresponds to that of MS stars with spectral type mid-F, and the equivalent widths of hydrogen absorption lines change significantly between spectra types F0V ( $M_K \sim 2$ ) to G0V ( $M_K \sim 3$ ). However, a change in  $\text{Br}\gamma - K$  colors due to spectroscopic variations among MS stars would be expected to occur over  $\sim 1$  magnitude in  $K$ , whereas the breaks found here seem to occur over a narrow magnitude range.

There is additional evidence that the changes in  $\text{Br}\gamma - K$  are due to PMS stars. There is a well-populated, narrow PMS sequence on the  $(K, J - K)$  CMD of NGC 3105, allowing PMS stars to be identified using their location on the CMD. The  $\text{Br}\gamma - K$  colors of objects

that fall along the PMS sequence can then be compared with those of objects that are not on this sequence, and so have a lower likelihood of being PMS stars. For the purposes of making such a comparison, objects in the interval  $K = 17.5$  and  $18.5$  that fall within  $\pm 0.15$  magnitude in  $J - K$  of the PMS sequence on the  $(K, J - K)$  CMD are assumed to be PMS objects, while those within the same  $K$  magnitude range but having  $J - K$  colors outside of the  $\pm 0.15$  magnitude PMS strip are classified as non-PMS objects.

If the PMS objects have  $\text{Br}\gamma$  photometric properties that differ on average from those of non-PMS stars then there should be statistically significant differences in  $\langle \text{Br}\gamma - K \rangle$ . The 122 objects in the PMS sample have  $\langle \text{Br}\gamma - K \rangle = -0.002 \pm 0.006$ , with a standard deviation  $\sigma = \pm 0.060$ . For comparison, the 66 non-PMS objects have  $\langle \text{Br}\gamma - K \rangle = 0.057 \pm 0.026$  with  $\sigma = \pm 0.221$ . The uncertainties in  $\langle \text{Br}\gamma - K \rangle$  are the  $1\sigma$  errors in the mean. The  $\langle \text{Br}\gamma - K \rangle$  of the PMS and non-PMS groups thus differ at the  $2\sigma$  level, in the sense that the PMS objects have a smaller  $\langle \text{Br}\gamma - K \rangle$ , and so are brighter in the  $\text{Br}\gamma$  filter than objects in the non-PMS sample that have the same  $K$ . A  $t$  test indicates that the means of the PMS and non-PMS samples differ at roughly the 98% confidence level, whereas an  $F$  test indicates that the standard deviations of these samples differ at more than the 95% confidence level. These comparisons thus indicate that the objects on the PMS sequence in the  $(K, J - K)$  CMD of NGC 3105 have photometric properties in the  $\text{Br}\gamma$  filter that differ systematically from those of non-PMS objects in the same  $K$  magnitude interval. The higher mean brightness in the  $\text{Br}\gamma$  filter for PMS objects is consistent with either line emission or weaker  $\text{Br}\gamma$  absorption.

The narrow-band  $\text{Br}\gamma$  observations identify NGC 2401 and NGC 3105 as interesting targets for follow-up observations. If  $\text{Br}\gamma$  emission is present then spectroscopy at visible/red wavelengths should reveal wide-spread  $\text{H}\alpha$  and  $\text{H}\beta$  emission from PMS objects in these clusters. The detection of line emission in a large fraction of the PMS objects would be astrophysically interesting, as it would indicate that they are actively accreting material.

Given that this activity would presumably have continued over the age of the clusters (20 – 30 Myr), then the lowest mass MS stars that ultimately form in these clusters may be more massive than those that form in clusters where accretion is truncated after a shorter period of time. If NGC 2401 and NGC 3105 are typical young outer disk clusters then the low mass portion of the IMF in this environment may differ from that in the solar neighborhood.

## 5. LUMINOSITY FUNCTIONS

The LFs of the clusters, corrected for field star contamination using number counts from the Robin et al. (2003) models, are shown in Figure 7. The predicted field star numbers were compared with source counts in the magnitude interval  $K = 12 - 15$  obtained from 2MASS images that sample areas around each cluster. Excellent agreement between the observed and predicted counts was found for NGC 2401. However, the models overestimate the field star numbers for the other two clusters by factors of  $1.30\times$  (Haffner 17) and  $1.16\times$  (NGC 3105). To correct the models for these discrepancies, the predicted field star counts for each cluster were scaled over all magnitudes by the same factor to force agreement with the 2MASS field star densities. Given the lack of checks on the numbers of field stars for magnitudes  $K \geq 15$  then the field star corrections are a source of uncertainty near the faint end of these data.

Also shown in Figure 7 are model LFs generated from the Bressan et al. (2012) isochrones. The models assume a coeval stellar content with a Chabrier (2001) lognormal MF, and a metallicity  $Z = 0.016$ . The first assumption is consistent with the modest age dispersion among stars in low mass (e.g. Hosokawa et al. 2011; Delgado et al. 2012; Bik et al. 2012) and at least some high mass (e.g. Kudryavtseva et al. 2012) clusters. The models have been scaled to match the observed number counts in the magnitude intervals indicated in each panel. The faint limit used for normalization was set at the same  $M_K$  for each cluster, whereas the bright limit was fixed at  $K = 14$ , as the number of stars in each

cluster plummets at brighter magnitudes than this.

**The artificial star experiments discussed in Section 3 indicate that the observations are complete for all clusters when  $K < 19.5$ , and so sample completeness is not an issue for the comparisons made in Figure 7.** The LF of Haffner 17 is flat, and is not matched by the models. The models fall  $\sim 1$  dex above the Haffner 17 LF at the faint end, indicating a substantial deficiency in low mass sources when compared with the Chabrier MF. The agreement between the models and observations would not be improved if a different magnitude interval was adopted for scaling the models.

The difference between the models and the observed counts in the upper panel of Figure 7 diminishes towards older ages, and better agreement could be obtained near  $K = 18$  if Haffner 17 were older than estimated here. However, the age of Haffner 17 would have to be in error by  $\geq 0.1$  Gyr to match the number of objects at  $K = 18$ , and this is unlikely given the location of the MSTO in the Pedredos (2000) CMD. Even then, a substantial disagreement between the models and number counts would remain at fainter magnitudes.

In contrast to Haffner 17, the model LFs match the NGC 2401 number counts over a large part of the LF. As NGC 2401 has the smallest fractional field star contamination, then its LF should be the least susceptible to uncertainties in field star contamination at the faint end. The models match the steady rise in number counts towards fainter magnitudes in NGC 2401 between  $K = 14$  and 16, which is the interval populated by bright MS stars. This agreement is consistent with the finding by Baume et al. (2006) that the MF of objects with masses  $\geq 1 M_{\odot}$  in NGC 2401 have a solar neighborhood-like MF. The LF of NGC 2401 flattens when  $K \geq 16$ , due to a change in the mass-luminosity relation of MS stars. This break is also reproduced by the models, and provides a loose check on the distance modulus.

The agreement between the models and the NGC 2401 LF is not so good for  $K > 16.5$ , with neither model providing a satisfactory match to the observations in this magnitude

range. Better agreement across the entire magnitude range could be obtained if the model normalization interval were extended to fainter magnitudes. Such a re-normalization would still produce agreement with the observations at the bright end within the error bars, although with the models falling systematically below the observations.

As for NGC 3105, there is statistical agreement between the models and the LF of this cluster near the bright end. Sagar et al. (2001) find that the bright members of NGC 3105 follow a MF with an exponent that is close to the Salpeter value, and the results in Figure 7 are consistent with this. However, statistically significant differences between the models and the NGC 3105 number counts occur in Figure 7 when  $K \geq 18.5$ . A broader normalization interval that encompasses fainter magnitudes would improve the agreement at the faint end slightly, although the quality of the fit at the bright end would then diminish.

In Section 4 it was demonstrated that the distance modulus computed from the  $(K, J - K)$  CMD depends on the metallicity of the isochrone that is compared with the CMD, and this could affect the agreement between the LFs and the models. NGC 3105 is the cluster in the present sample that is most likely to have a sub-solar metallicity given its large  $R_{GC}$ . The green curves in the lower panel of Figure 7 show the result of adopting a distance modulus that is 0.15 dex smaller (i.e. corresponding to what would be obtained from an isochrone with a metallicity that is 1/2 Solar – Section 4) for NGC 3105. The agreement between the observations and the models does not change greatly when this lower distance modulus is applied. The conclusions reached in this section are thus not sensitive to uncertainties in the adopted distance moduli.

In addition to providing insight into the MF, the LF of a star cluster also contains information about its age. The trajectory of the PMS sequences in Figures 1 - 3 tend to flatten near the MSCO, resulting in a build-up of PMS objects in a narrow magnitude interval, creating a bump in the LF that can be used as an age indicator (e.g. Cignoni et al. 2010; Davidge 2012). The ability to detect this feature depends on factors such as age,



the number of stars, and the binning used to construct the LFs. Cignoni et al. (2010) argue that this feature is a useful age indicator for well-populated systems that are younger than  $\sim 30$  Myr.

Can the LFs in Figure 7 be used to place constraints on the cluster ages? Haffner 17 is not considered when answering this question given the difficulty matching the overall shape of the cluster LF. As for NGC 2401, if it has an age  $\log(t_{yr}) = 7.4$  then the model predicts that there should be a PMS bump near  $K = 17$ , while for an age  $\log(t_{yr}) = 7.6$  then the bump is 0.5 magnitudes fainter. The NGC 2401 LF does not contain a feature at either magnitude, although the amplitudes of the bumps in the models are comparable to the error bars in the LF. While the dip in number counts between  $K = 16.5$  and  $K = 17$  might be consistent with an age  $\log(t_{yr}) \sim 7.2$ , the statistical significance of this feature is low. There are no obvious signatures of a PMS-related bump in the NGC 3105 LF. These comparisons suggest that the PMS bump is only a useful age indicator for systems that are more massive than NGC 2401 and NGC 3105 (i.e. masses  $> 5 \times 10^2 M_{\odot}$ ).

## 6. THE CORRELATION PROPERTIES OF CLUSTER STARS

The spatial distribution of stars in a cluster evolves with time as the system relaxes. However, non-secular processes may also affect the spatial distribution of cluster stars. For example, the expulsion of large quantities of gas early in the life of a system due to winds and/or supernovae (SNe) will change the gravitational potential. The system will expand (e.g. Baumgardt & Kroupa 2007), and stars with velocities that exceed the new (lower) escape velocity of the mass-depleted system will be lost.

The clustering properties of three samples of objects in Haffner 17, NGC 2401, and NGC 3105 are examined: (1) all detected objects (the ‘ALL’ sample), (2) bright main sequence stars (the ‘BMS’ sample), which have  $M_K \leq 2.5$  and are on the MS, and (3) faint main

sequence/ pre-main sequence objects (the ‘FMS’ sample), which have  $M_K$  between 3 and 5. Absolute magnitudes were computed using the distance moduli obtained in Section 4. The degree of clustering is measured with the two-point angular correlation function (TPCF). The core component of the TPCF is the separation function (SF), which is the distribution of separations between all possible source pairings. The SF multiplexes information from all objects, and so makes efficient use of available information, although at the price of mixing information from cluster and non-cluster members. Geometric effects are rectified by dividing the SF by that of an artificially-generated uniformly-distributed sample of objects with an image geometry that mimics the actual data. This ratio is then normalized according to the number of pairings in the two SFs.

The TPCFs of the ALL samples are compared in the top panel of Figure 8. The TPCFs reflect the clustering properties of a mix of cluster members and field stars, and the impact on field star contamination on the TPCFs is examined later in this section. Still, the TPCFs of the cluster ALL samples are similar over most separations, with uniform clustering properties for separations between 20 and 40 arcsec. The TPCFs of the ALL samples diverge at separations  $> 76 - 80$  arcsec.

The TPCFs of the ALL samples differ at small separations, and this may signal differences in the binary star contents. Binaries in nearby star-forming regions have separations  $< 0.04$  pc (Larson 1995), and the widest such binaries are resolved with these data in all three clusters. However, cluster-to-cluster comparisons are complicated by differences in the distance and angular resolution. Consider Haffner 17, where there is a peak in the TPCF at the smallest separations in the upper panel of Figure 8. The bin that covers the smallest separations samples objects with spatial separations from 0.0024 pc (i.e. 0.12 arcsec – the angular resolving power of the data) to 0.04 pc (i.e. 2 arcsec - the bin size used to construct the TPCF). The bin that samples the smallest separations in Haffner 17 thus covers a clean population of binaries. In contrast, NGC 3105 is the most distant cluster, and the smallest

separation bin in that cluster samples objects with projected separations of 0.0063 – 0.070 pc. Therefore, binaries at spatial separations that would be detected in Haffner 17 are not resolved in NGC 3105, and the binary signal in NGC 3105 is diluted by non-binaries in the smallest separation bin.

The clustering properties of stars having different masses – such as the objects in the BMS and FMS samples – provide insights into the dynamical state of a system. For example, objects with lower masses being more uniformly distributed on the sky than higher mass objects is a signature of mass segregation, although other processes could produce similar results. The ratio of the SFs of the BMS and FMS samples are shown in the lower panel of Figure 8. If the objects in the BMS and FMS samples have similar clustering properties then the ratio of the SFs should be  $\sim 1$ , and this is the case over most separations in NGC 2401. Significantly, the LF of NGC 2401 was also found to be similar to the solar neighborhood (Section 5). If it is assumed that the MF is universal then this suggests that mass segregation is not yet well advanced in the mass range probed in NGC 2401.

The situation is different for Haffner 17 and NGC 3105. While the ratio of the BMS and FMS SFs is close to unity in both clusters for separations  $< 60$  arcsec, this is not the case at higher separations. This behaviour indicates that sources in the FMS samples are more uniformly distributed across the GSAOI field over large angular scales than the objects in the BMS samples. However, field star contamination is substantial in both clusters, and this must be considered when interpreting these results.

Field stars are uniformly distributed on the sky and will bias TPCFs towards flatter distributions. If the magnitude intervals that cover the BMS and FMS samples have different fractional contaminations from field stars then the ratio of the BMS and FMS SFs will be skewed by these differences. The field star fraction in the Haffner 17 and NGC 3105 data is higher in the FMS sample (70% in Haffner 17 and 64% in NGC 3105) than in the BMS sample (29% in Haffner 17 and 41% in NGC 3105). For comparison, the field star fraction in

the NGC 2401 BMS and FMS samples – where the objects show similar clustering properties (see above) – are not greatly different, with 26% contamination in the BMS sample, and 29% in the FMS sample.

It is difficult to separate cluster and field stars in the absence of proper motion and radial velocity measurements. However, the role that field stars play in the BMS and FMS samples can be assessed in a statistical manner. Following the procedure described by Davidge et al. (2013), objects that have a uniform on-sky distribution – thereby simulating the distribution of field stars – were added to the BMS samples of Haffner 17 and NGC 3105 to boost artificially the field star fraction to match that in the corresponding FMS samples. A number of realizations were run, and a mean BMS+field star SF was computed for both clusters to suppress stochastic variations. The results are compared with the observed BMS TPCFs in the top panel of Figure 9.

Introducing a simulated field star population has only a modest impact on the BMS TPCFs at small separations, reflecting the modest on-sky density of the added stars, and the resulting low probability that they are near other objects. However, the multiplexed nature of the SFs causes the contribution made by the added stars to grow towards progressively larger separations. It can be seen in Figure 9 that balancing the field star fractions affects the TPCFs at separations  $> 60$  arcsec, which is where differences between the BMS and FMS samples of Haffner 17 and NGC 3105 in Figure 8 are apparent.

The ratios of the mean BMS+field star and FMS TPCFs of Haffner 17 and NGC 3105 are shown in the lower panel of Figure 9. Balancing the field star levels in the BMS and FMS samples moves the ratio of TPCFs at separations  $> 60$  arcsec in Haffner 17 much closer to unity, as expected if the differences in Figure 8 between the Haffner 17 samples are significantly skewed by field stars. Still, it is apparent that the BMS and FMS samples in this cluster have different angular distributions, as the BMS/FMS ratio falls consistently below unity at separations  $> 80$  arcsec after balancing the field star fractions. As for NGC

3105, the FMS sample also remains more uniformly distributed than the BMS component after balancing the field star fractions. There are thus mass-related differences in the spatial distribution of stars in Haffner 17 and NGC 3105. This is evidence that these clusters are dynamically evolved.

## 7. DISCUSSION & SUMMARY

Near-infrared images obtained with GSAOI+GeMS have been used to examine the photometric properties and spatial distributions of stars in the young open clusters Haffner 17, NGC 2401, and NGC 3105. These clusters are located at large Galactocentric radii, and NGC 3105 is one of the most remote young clusters yet discovered in the Galaxy. Studies of external galaxies suggest that young and intermediate age clusters are not uncommon in the outermost regions of star-forming disks (e.g. Herbert-Fort et al. 2012). Studies of young clusters in the outer Galaxy may then yield insights into how clusters in the outer disks of spiral galaxies evolve in general. Because these clusters are in an environment that is systematically different from the Solar Neighborhood, their evolution might differ from those of better-studied nearby clusters.

The age, reddening, and distance modulus estimated for each cluster from the GSAOI+GeMS data are summarized in Table 3. The distances and reddenings found here are based on the morphology of the MS on the  $(K, J - K)$  CMD. The distances measured for NGC 3105 and NGC 2401 place them closer than previous studies, while the opposite is true for Haffner 17. The reddenings of all three clusters also differ from previous estimates. It should be recalled that the  $E(B - V)$  values found here were computed from  $E(J - K)$  using the entries in Table 6 of Schlegel et al. (1998). If the extinction along the lines of sight to the target clusters follows different reddening laws then this will affect comparisons with  $E(B - V)$  estimates made at visible wavelengths.

The ages are based on the photometric properties of PMS and lower mass MS stars, and so are independent of previous age estimates that relied on the MSTO. Barring a peculiar MF, ages that rely on faint cluster members will be less susceptible to the statistical variations in stellar content that can affect the brightest MS and evolved stars in low mass clusters, which in turn complicates efforts to determine ages from the MSTO. This being said, the use of faint objects to measure ages comes at a cost. Uncertainties in the photometric measurements increase towards fainter magnitudes, and sample completeness may become a factor when assessing the magnitude of the MSCO. Contamination from field stars also becomes a concern when measuring ages from faint members, as the number of field stars grows towards fainter magnitudes. The predominantly red colors of field stars also mean that they will tend to overlap more with those of PMS stars than with stars near the MSTO. Finally, there are also numerous uncertainties in models of PMS objects (e.g. Seiss 2001). Still, it is encouraging that the isochrones used here track the observed PMS sequences, and yield ages that are consistent with previous determinations.

Haffner 17 has the most sparsely populated CMD in our sample, and so it might be anticipated that the age measured from the MSTO of that cluster will be the most prone to statistical variations among the brightest MS stars. However, there is no evidence that this is the case, as the age determined from the GSAOI data is consistent with that found by Pedredos (2000). As for NGC 2401 and NGC 3105, the GSAOI data suggest that these clusters have ages 20 – 30 Myr. Previous studies of NGC 2401 have suggested a wide range of ages, and our results favor the age found by Baume et al. (2006), as opposed to those measured by Sujatha et al. (2004) and Hasegawa et al. (2008). The age measured for NGC 3105 agrees with those deduced by Sagar et al. (2001) and Paunzen et al. (2005) from the MSTO. The good agreement with published ages suggests that stochastic effects have not affected the present-day MSTO contents of these clusters.

Given their ages, the clusters are expected to contain faint sub-solar mass PMS objects,

and PMS sequences are seen in the CMDs of NGC 2401 and NGC 3105. An intriguing result from Section 4 is that the mean  $\text{Br}\gamma - K$  color changes within  $\sim 0.6$  magnitudes in  $K$  of the onset of the PMS sequence in both clusters. In addition, the photometric properties of stars along the PMS sequence in NGC 3105 differ from those of field stars in the same magnitude interval, in the sense that the PMS stars are brighter on average in the  $\text{Br}\gamma$  filter at a given  $K$  magnitude than field stars. While narrow-band  $\text{Br}\gamma$  observations alone do not provide the information required for an unambiguous interpretation of the cause of these differences, both results are consistent with  $\text{Br}\gamma$  emission being present. Optical and/or near-infrared spectroscopy will be required to determine if line emission is present. If  $\text{Br}\gamma$  emission is present among PMS stars in NGC 2401 and NGC 3105 then it must have a high frequency of occurrence to affect the mean  $\text{Br}\gamma - K$  colors.

Star clusters disperse in response to internal and external processes. Despite having more-or-less similar ages, our data suggest that Haffner 17, NGC 2401, and NGC 3105 are in different stages of evolution. The  $K$  LFs discussed in Section 5 provide some of the evidence that supports this interpretation. The  $K$  LF of NGC 2401 is well-matched over a wide magnitude range by models that assume a Chabrier (2001) MF. To the extent that the initial MF of stars having masses within a few tenths of a dex of solar is universal, then this suggests that NGC 2401 has not shed large numbers of low mass stars. However, this is not the case for NGC 3105, as the  $K$  LF of this cluster is deficient in low mass objects when compared with models. The  $K$  LF of Haffner 17 is very different from those of either NGC 2401 and NGC 3105, in that it is relatively flat, even at the bright end.

The spatial distributions of MS and PMS stars provide additional evidence that the clusters are in different stages of evolution. BMS and FMS objects in NGC 2401 have similar clustering properties, suggesting that intermediate and low mass objects in NGC 2401 have not yet developed kinematically distinct distributions, and this is further evidence that NGC 2401 is not dynamically evolved. In contrast, after balancing field star contamination in

different magnitude intervals, PMS objects and low mass MS stars in Haffner 17 and NGC 3105 are more uniformly distributed than stars in the BMS sample, suggesting that low and high mass objects in these clusters have different kinematic properties.

Insights into the evolutionary status of these clusters can also be deduced from their integrated properties. Cluster masses, radii, and free-fall times were calculated for each cluster, and the results are shown in Table 3. The masses were computed by transforming the cluster LFs into MFs using magnitude *vs* mass relations from the Padova isochrones, and then integrating the results. These masses are lower limits because (1) the clusters extend beyond the GSAOI field, and (2) cluster members with masses  $\leq 0.3 M_{\odot}$  are not sampled with these data. Still, the corrections for these effects are likely to be modest. An alternative would be to compute total masses from the integrated brightnesses listed in Table 1, although the results would be highly uncertain due to the presence of bright stars (Section 1).

The last column of Table 3 lists the ratio of the cluster age to the dynamical time scale ( $\tau_{dyn}$ ), which is one measure of the kinematic state of a system. Marks & Kroupa (2012) find that significant evolution in cluster density occurs when a system is younger than  $\sim 10\tau_{dyn}$ , and that only more subdued changes in density occur after this time. To the extent that the ratio of cluster age to the dynamical timescale is a simple probe of kinematic evolution, it indicates that NGC 2401 is the least evolved cluster (i.e. it has the smallest ratio of age to  $\tau_{dyn}$ ). This is consistent with the investigation of the MF and the angular distributions of BMS and FMS stars presented above. In contrast, Haffner 17 and NGC 3105 are predicted to be more evolved than NGC 2401.

If these clusters formed in large-scale complexes then they may be susceptible to environmentally-driven evolution. However, an examination of Digital Sky Survey images shows that the clusters are isolated, in the sense that neighboring stellar groupings are at least 10 arcmin away in projection. Of course, over tens of Myr the random motions that



clusters attain in disks may cause them to move large distances and erase structure that was in place during the time of their formation (e.g. Davidge 2007). Their present-day environment may then be very different from the environment where they formed.

The evolution and present-day appearance of a cluster can also be shaped early in its life by internally-driven events that can cause significant cluster-to-cluster differences in stellar content. Systems that form massive, short-lived stars may be prone to a catastrophic loss of gas driven by winds and SNe that can change the gravitational potential and cause the cluster to disperse (e.g. Lada & Lada 2003). If SNe activity is delayed then the likelihood of a cluster being disrupted will drop, as the fraction of cluster mass that is in gas and dust decreases with time as this material is consumed by star formation and disperses from the cluster – as time passes the removal of gas will then have a smaller impact on the cluster potential. Any delay in SNe activity also allows cluster members to come closer to being fully virialized, with the result that the extremes in velocity that are conducive to the loss of stars when the cluster potential changes are reduced (e.g. Smith et al. 2011).

The total stellar mass of a cluster likely plays a key role in determining if internal processes drive its evolution. Pelupessy & Portegies Zwart (2012) investigate the role that statistical variations among massive stars play in the evolution of systems with stellar masses  $\sim 350 M_{\odot}$ . The three clusters studied here have masses close to that adopted for the simulations, allowing relevant comparisons to be made. Pelupessy & Portegies Zwart find that stochastic variations in the population of upper MS stars can lead to profound cluster-to-cluster differences in the early evolution of the simulated clusters. If stars are present that are massive enough to become SN early-on, then low mass stars – which attain higher velocities than more massive stars as a system relaxes – may be preferentially lost from the cluster early in its evolution. On the other hand, if statistical fluctuations in stellar content are such that very massive stars do not form then a cluster may not be purged of gas until much later in its life, with a smaller impact on its structural characteristics. Of course, the

timing of SNe activity is not the only factor that shapes early cluster evolution. For example, sub-clustering may concentrate star-forming activity, lowering local gas fractions and thus reducing the impact of SNe-driven gas loss (Kruijssen et al. 2012).

The properties of the NGC 2401 LF and the relative distributions of its stars in the BMS and FMS samples hint that NGC 2401 was not subjected to violent early evolution, and had an uneventful past. However, the same can not be said for Haffner 17 and NGC 3105, and there are observations that could be carried out that would cast light on their early histories. Clusters will expand in response to the sudden loss of large quantities of gas (e.g. Baumgardt & Kroupa 2007), and an extended stellar halo might be an observational signature of this (e.g. Davidge 2012; Bastian & Goodwin 2006). If Haffner 17 and NGC 3105 experienced early mass loss then a wide-field survey of these clusters may reveal a halo containing objects that span a range of masses, although the long term survivability of such a structure will depend on the local tidal field. In the case of NGC 3105 some of the halo objects should be PMS sources, and these may not be difficult to detect if they are hydrogen line emitters, as suggested in Section 4.

In addition to affecting the structural properties of star clusters, the presence of massive hot stars may also affect the final MF of stars that form. The ultraviolet radiation field produced by very massive stars may erode nearby accretion disks and choke subsequent stellar growth, thereby affecting the minimum stellar mass in their immediate vicinity (e.g. Johnstone et al. 1998; Adams et al. 2004; De Marchi et al. 2011). If Haffner 17 contained an extremely massive hot star then such an object may have affected the final cluster MF.

The preceding discussion assumes that the processes that drive the disruption of a cluster during the initial stages of its assembly differ from those that disrupt older clusters. However, there are hints that the disruption rate of very young clusters may be similar to that of older clusters, as would be expected if cluster destruction during the early stages of cluster assembly and at later times are driven by the same mechanisms. In particular, if all

stars form in clusters, then the relative numbers of stars that are in clusters and the field in the Solar neighborhood suggest that over 90% of natal groupings are disrupted within 10 Myr of their birth (Bonatto & Bica 2011). If it is assumed that clusters remain intact over the lifetimes of their most massive stars (i.e.  $\sim 1$  Myr), then this pace of attrition is consistent with that seen among clusters that span a broad range of ages in nearby disk galaxies, where the number of clusters drops by roughly an order of magnitude for every decade in age (Fall & Chandar 2012). That the pace of cluster destruction among very young systems tracks that among much older systems is suggestive of similar mechanisms disrupting clusters over a wide range of ages. If this is the case then while very young clusters are undoubtedly subject to mass loss driven by winds and SNe, these may not be the dominant mechanisms driving cluster disruption.

Thanks are extended to the anonymous referee for providing a prompt and helpful report.

Cluster	$\ell$ (Degrees)	$b$ (Degrees)	$\log(\text{age})^1$ (years)	$\mu_0^1$	$K_{Tot}^2$	Radius <sup>2</sup> (arcsec)	$M_K^{Tot}$
Haffner 17	247.7	-2.5	7.7	12.3	7.3	75	-5.0
NGC 2401	229.7	1.9	7.4	14.0	10.7	45	-3.3
NGC 3105	279.9	0.3	7.2	13.4	5.6	80	-7.8

Table 1: Cluster Parameters

<sup>1</sup>From August 2013 version of WEBDA database.

<sup>2</sup>Measured from 2MASS images.

Cluster	Date Observed	$r_0^1$ (cm)	$\langle R \rangle^2$	Filter (sec)	Exposure Times (arcsec)	$\langle FWHM \rangle^3$ (arcsec)	$\sigma_{FWHM}^4$
Haffner 17	Jan 29, 2013	13.0	13.8	J	$3 \times 10; 5 \times 25$	0.119	$\pm 0.012$
				Ks	$3 \times 10; 5 \times 25$	0.098	$\pm 0.005$
				Br $\gamma$	$3 \times 10; 5 \times 60$	–	–
NGC 2401	Jan 30, 2013	11.0	14.3	J	$3 \times 10; 5 \times 40$	0.093	$\pm 0.010$
				Ks	$3 \times 5; 5 \times 25$	0.083	$\pm 0.007$
				Br $\gamma$	$3 \times 5; 5 \times 60$	–	–
NGC 3105	Jan 26, 2013	9.0	11.5	J	$3 \times 10; 5 \times 40$	0.178	$\pm 0.017$
				Ks	$3 \times 10; 5 \times 40$	0.117	$\pm 0.012$
				Br $\gamma$	$3 \times 10; 5 \times 60$	–	–

Table 2: Details of the Observations

<sup>1</sup>Fried parameter at  $\lambda = 500$  nm measured at the mid-point of the cluster observing sequence.

<sup>2</sup>Mean R magnitude of NGSs.

<sup>3</sup>Mean FWHM measured from the PSF stars in the long exposure images.

<sup>4</sup>Standard deviation about  $\langle FWHM \rangle$ .

Cluster	Age <sup>1</sup> (Myr)	E(B-V) <sup>1</sup>	$\mu_0$ <sup>1</sup>	Mass (M <sub>⊙</sub> )	Radius (pc)	$\tau_{dyn}$ <sup>2</sup> (Myr)	Age/ $\tau_{dyn}$
Haffner 17	52	0.85	13.0	270	1.7	3.2	16
NGC 2401	25	0.15	13.7	230	1.2	2.0	12
NGC 3105	25	0.70	14.3	490	2.8	1.5	17

Table 3: Cluster Properties

<sup>1</sup>Values found in this study. The ages quoted for Haffner 17 and NGC 2401 are the midpoints of the age ranges estimated in Section 4.2.2.

<sup>2</sup>Dynamical timescale.

## REFERENCES

- Adams, F. C., Hollenbach, D., Laughlin, G., & Gorti, U. 2004, *ApJ*, 611, 360
- Balsler, D. S., Rood, R. T., Bania, T. M., & Anderson, L. D. 2011, *ApJ*, 738, 27
- Bastian, N., & Goodwin, S. P. 2006, *MNRAS*, 389, 223
- Baume, G., Moitinho, A, Vazquez, R. A., Solivella, G., Carraro, G., & Villanova, S. 2006, *MNRAS*, 367, 1441
- Baumgardt, H., & Kroupa, P. 2007, *MNRAS*, 380, 1589
- Bik, A., Henning, Th., Stolte, A., et al. 2012, *ApJ*, 744, 87
- Bonatto, C., & Bica, E. 2011, *MNRAS*, 415, 2827
- Bressan, A., Marigo, P., Girardi, L., Salasnich, B., Dal Caro, C., Rubele, S., & Nanni, A. 2012, *MNRAS*, 427, 127
- Carrasco, E. R., Edwards, M. L., McGregor, P. S. et al. 2012, *SPIE*, 8447, E0
- Chabrier, G. 2001, *ApJ*, 554, 1274
- Cignoni, M., Tosi, M., Nota, A., et al. 2010, *ApJ*, 712, L63
- Davidge, T. J. 2007, *ApJ*, 664, 820
- Davidge, T. J. 2012, *ApJ*, 761, 155
- Davidge, T. J., Carrasco, E. R., Winge, C., Pessev, P., Neichel, B., Vidal, F., & Rigaut, F. 2013, *PASP*, in press
- Delgado, A. J., Alfaro, E. J., & Yun, J. L. 2011, *A&A*, 531, A141
- De Marchi, G., Panagia, N., Romaniello, M., Saba, E., Sirianni, M., Prada Moroni, P. G., & Degl’innocenti, S. 2011, *ApJ*, 740, 11
- Donehew, B., & Brittain, S. 2011, *AJ*, 141, 46
- Fall, S. M., & Chandar, R. 2012, *ApJ*, 752, 96

- Fitzgerald, M. P., Jackson, P. D., & Moffat, A. F. J. 1977, *A&A*, 59, 141
- Fried, D. L. 1966, *JOSA*, 56, 1372
- Hasegawa, T., Sakamoto, T., & Malasan, H. L. 2008, *PASJ*, 60, 1267
- Herbert-Fort, S., Zaritsky, D., Moustakas, J., Di Paola, A., Pogge, R. W., & Ragazzoni, R. 2012, *ApJ*, 754, 110
- Hosokawa, T., Offner, S. S. R., & Krumholz, M. R. 2011, *ApJ*, 738, 140
- Johnstone, D., Hollenbach, D., & Bally, J. 1998, *ApJ*, 499, 758
- Kruijssen, J. M. D., Maschberger, T., Moeckel, N., Clarke, C. J., Bastian, N., & Bonnell, I. A. 2012, *MNRAS*, 419, 841
- Kudryavtseva, N., Brandner, W., Gennaro, M., et al. 2012, *ApJ*, 750, L44
- Lada, C. J., & Lada, E. A. 2003, *ARA&A*, 41, 57
- Larson, R. B. 1995, *MNRAS*, 272, L213
- Marks, M., & Kroupa, P. 2011, *MNRAS*, 417, 1702
- Marks, M., & Kroupa, P. 2012, *A&A*, 543, A8
- McGregor, P., Hart, P., John, S. et al. 2004, *SPIE*, 5492, 1033
- Mermilliod, J.-C. 1995, in *Information and On-Line Data in Astronomy*, ed. D. Egret & M. A. Albrecht (Dordrecht: Kluwer), 127
- Moffat, A. F. J., & Fitzgerald, M. P. 1974, *A&AS*, 16, 25
- Neichel et al. 2012, *SPIE*, 8447, 84474
- Paunzen, E., Netopil, M., Iliev, I. K., Maitzen, H. M., Claret, A., & Pintado, O. I. 2005, *A&A*, 443, 157
- Pedredos, M. H. 2000, *Rev. Mex. A. & Ap.*, 26, 13
- Pelupessy, F. I., & Portegies Zwart, S. 2012, *MNRAS*, 420, 1503



- Rigaut et al. 2012, SPIE, 8447, 84470
- Robin, A. C., Reyle, C., Derriere, S., & Picaud, S. 2003, A&A, 409, 523
- Sagar, R., Munari, U., & de Boer, K. S. 2001, MNRAS, 327, 23
- Schlegel, D. J., Finkbeiner, D. P., & Davis, M. 1998, ApJ, 500, 525
- Seiss, L. 2001, in ASP Conf. Ser. 243, From Darkness to Light, ed. T. Montmerle & P. André (San Francisco, CA: ASP), 581
- Silva-Villa, E., & Larsen, S. S. 2011, A&A, 529, A25
- Smith, R., Fellhauer, M., Goodwin, S., & Assmann, P. 2011, MNRAS, 414, 3036
- Stetson, P. B. 1987, PASP, 99, 191
- Stetson, P. B., & Harris, W. E. 1988, AJ, 96, 909
- Sujatha, S., Babu, G. S. D., & Ananthamurthy, S. 2004, Bull. Astr. Soc. India, 32, 295
- Vernin, J., Agabi, A., Avila, R., Azouit, M., Conan, R., Martin, F., Masciadri, E., Sanchez, L., & Ziad, A. 2000, ‘Gemini CP Site Characterization Report’, GEMINI RPT-AO-G0094

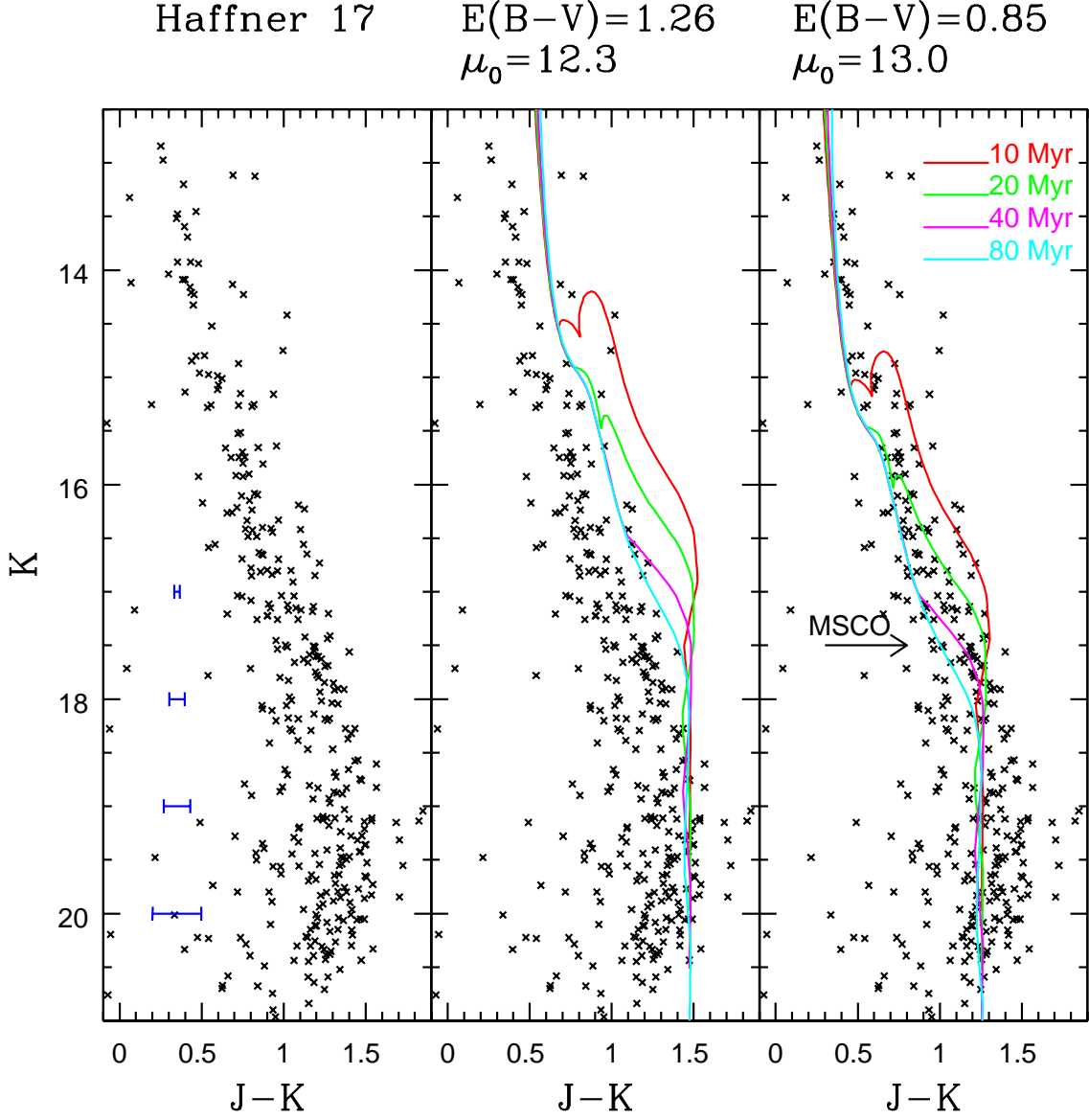


Fig. 1.— The  $(K, J - K)$  CMD of Haffner 17 is compared with  $Z = 0.016$  isochrones from Bressan et al. (2012). **The blue error bars in the left hand panel are the  $\pm 1\sigma$  random uncertainties calculated from artificial star experiments.** The comparisons in the middle panel use the reddening and distance modulus determined by Pedredos (2000), while those in the right hand panel use the reddening and distance modulus found here. The approximate location of the MS cut-off (MSCO), determined in Section 4.2, is indicated in the right hand panel.

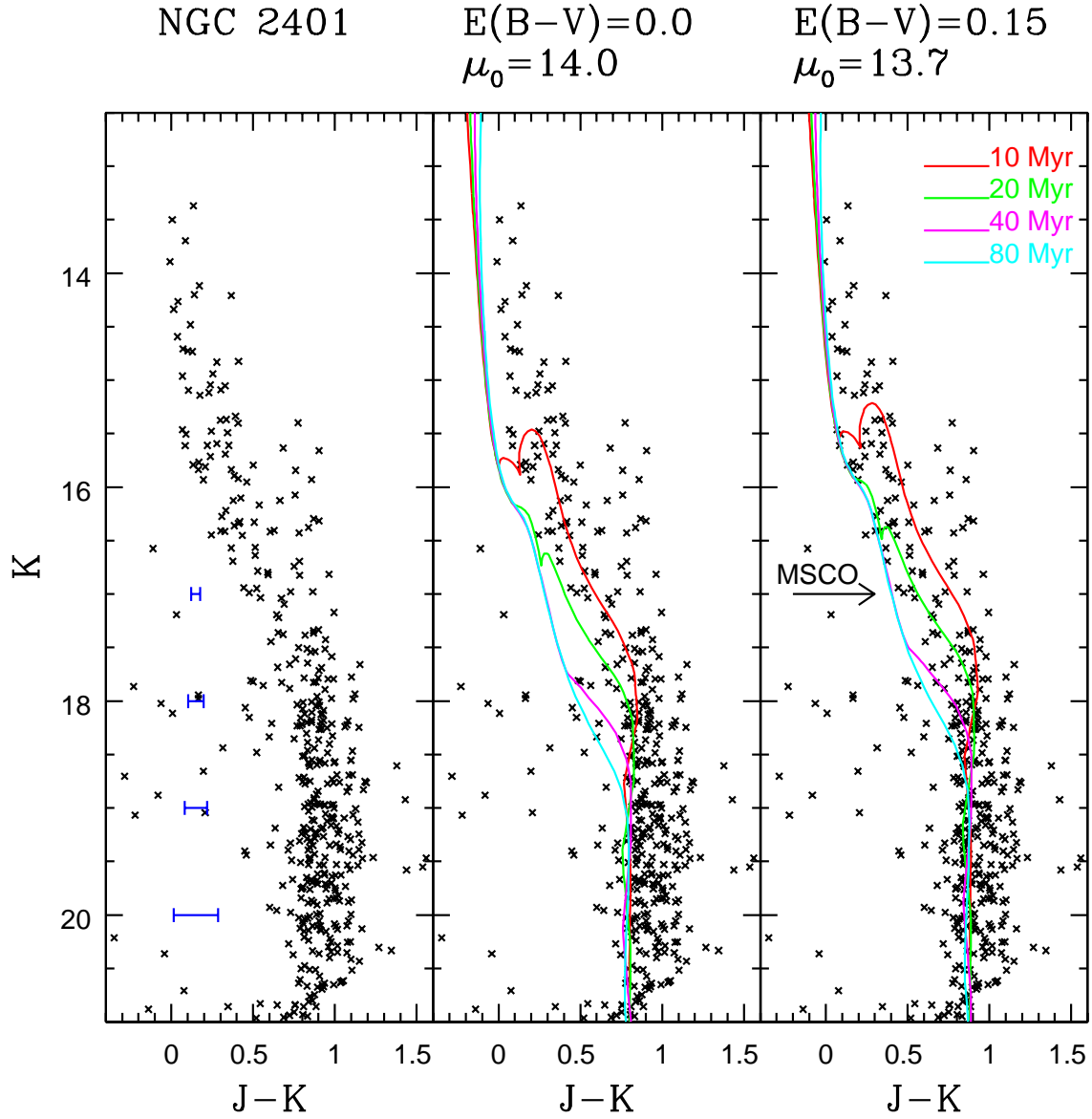


Fig. 2.— The same as Figure 1, but for NGC 2401. The reddening and distance modulus used in the middle panel are from Baume et al. (2006).

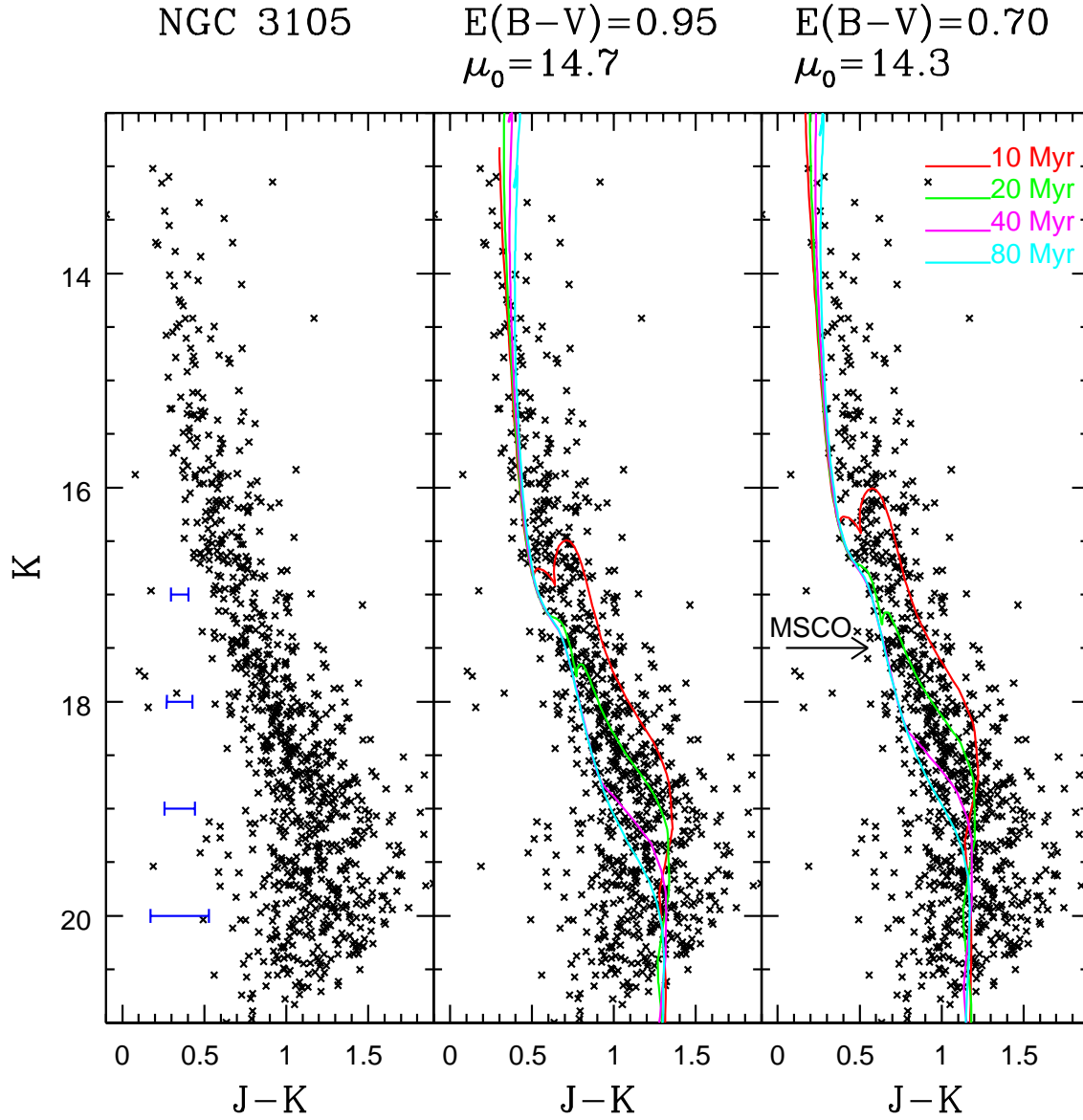


Fig. 3.— The same as Figure 1, but for NGC 3105. The reddening and distance modulus used in the middle panel are from Paunzen et al. (2005).

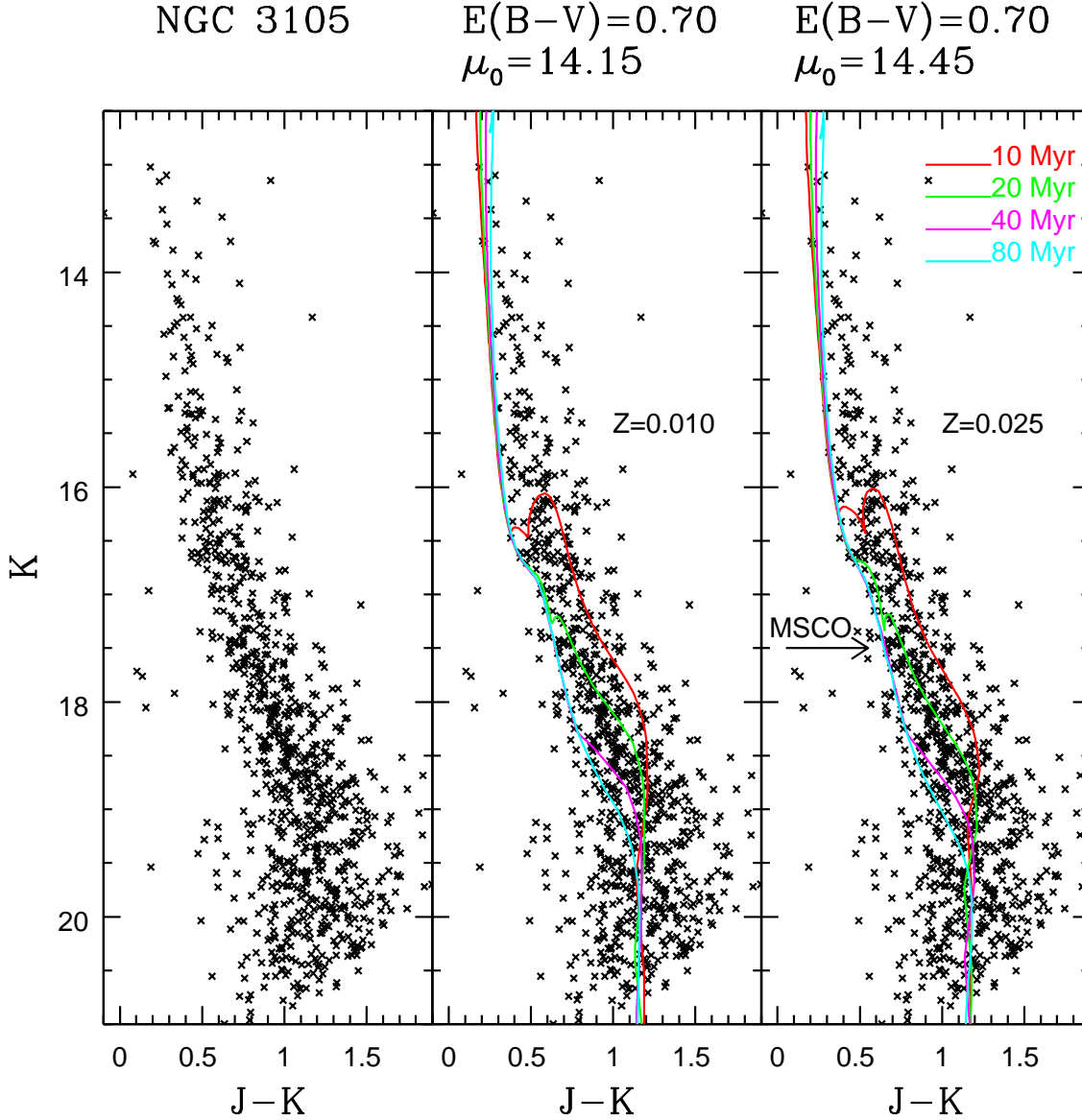


Fig. 4.— The sensitivity of the measured distance and reddening to metallicity. The  $(K, J-K)$  CMD of NGC 3105 is compared with  $Z = 0.010$  and  $Z = 0.025$  isochrones in the middle and right hand panels.  $E(B-V)$  and  $\mu_0$  have been estimated for both metallicities using the criteria employed for the comparison in the right hand panel of Figure 3. The same reddening is found for both metallicities. However,  $\mu_0$  differs by 0.30 dex, in the sense of larger  $\mu_0$  values as metallicity increases. Significantly, the PMS sequence that runs from  $K = 17.5$  to 19 is paralleled by the 20 Myr isochrones for both metallicities, and is consistent with an age  $\sim 25$  Myr.

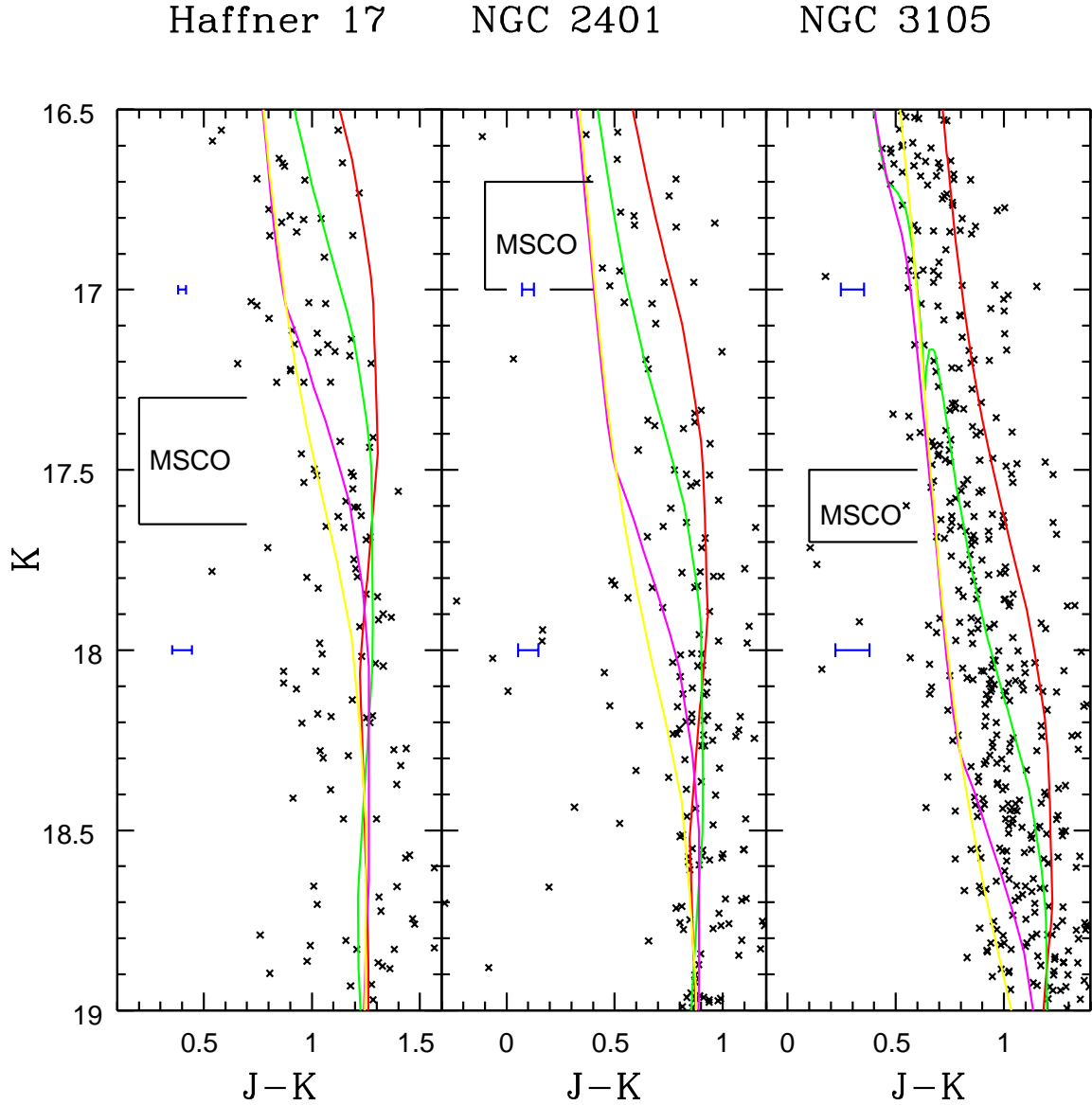


Fig. 5.— The sections of the CMDs containing the lower portions of the MS and the upper portions of the PMS. **The blue error bars show the  $\pm 1\sigma$  random uncertainties in  $J - K$  calculated from the artificial star experiments.** Bright and faint limits for the MSCO are indicated for each cluster, and the criteria for selecting these are discussed in the text. The red, green, and violet lines are isochrones with the same color codes used in Figures 1 – 4, while the yellow sequence is a 1 Gyr isochrone with  $Z = 0.016$ . The CMDs of NGC 2401 and NGC 3105 contain sequences that are populated by PMS stars. The PMS sequence of NGC 2401 is well matched by the 20 Myr isochrone, whereas the PMS locus of NGC 3105 is consistent with an age 25 Myr.

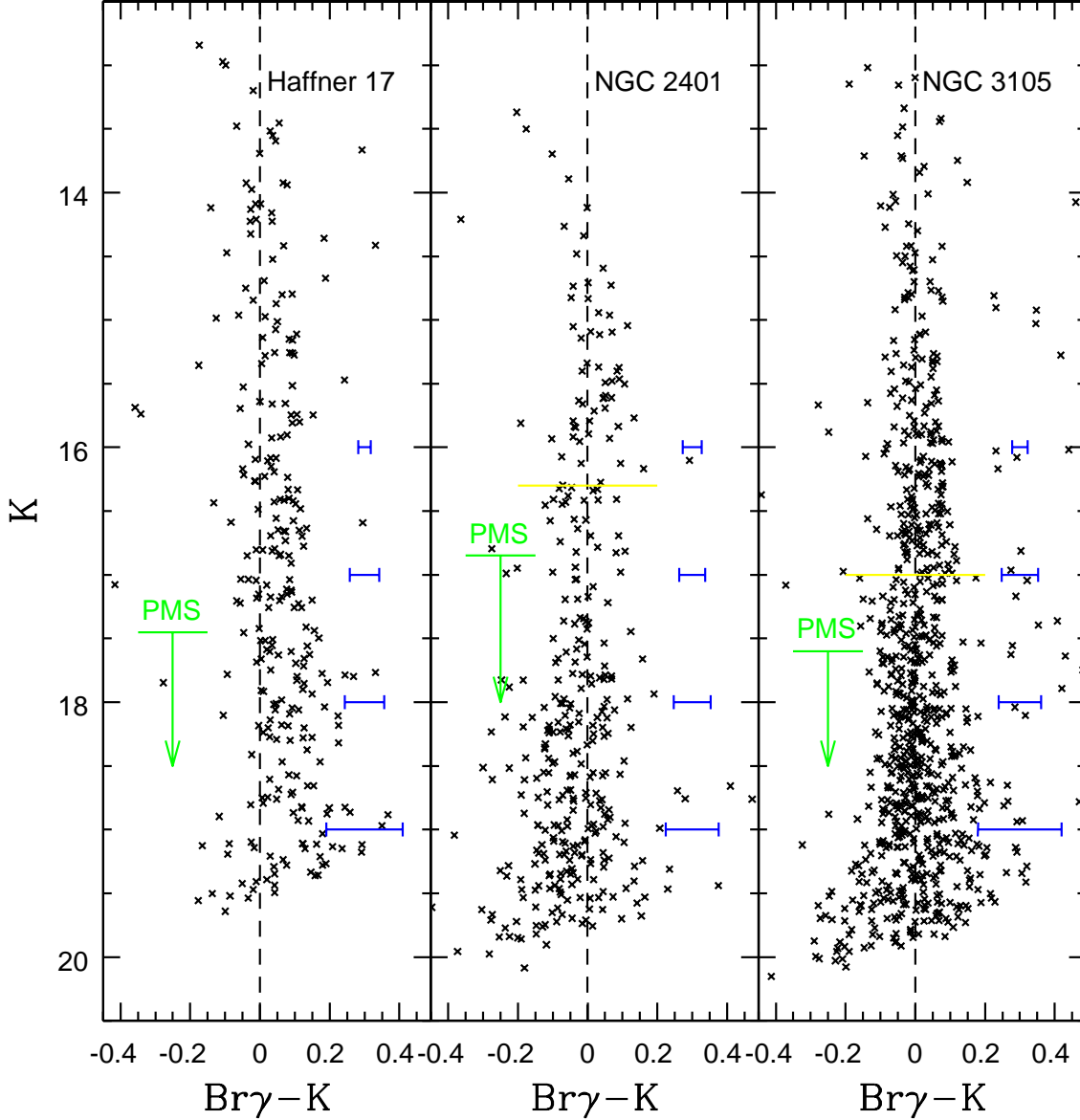


Fig. 6.—  $(K, Br\gamma - K)$  CMDs. The dotted line indicates  $Br\gamma - K = 0$ , and the magnitude range where PMS stars are expected is shown for each cluster. The blue error bars show the  $\pm 1\sigma$  random dispersion in the photometry calculated from artificial star experiments. The  $(K, Br\gamma - K)$  CMD of Haffner 17 does not show obvious changes near the MSCO. In contrast, breaks in the  $Br\gamma - K$  colors of NGC 2401 and NGC 3105 occur near  $K = 16.3$  (NGC 2401) and  $K = 17$  (NGC 3105), and these breaks are indicated with the yellow lines. The artificial star experiments indicate that the data for both clusters are complete at these magnitudes, and that the breaks are not due to systematic errors in the photometry. Kolmogorov-Smirnov tests indicate that the  $Br\gamma - K$  distributions of objects in intervals above and below these points differ at the 95%+ confidence level in both clusters.

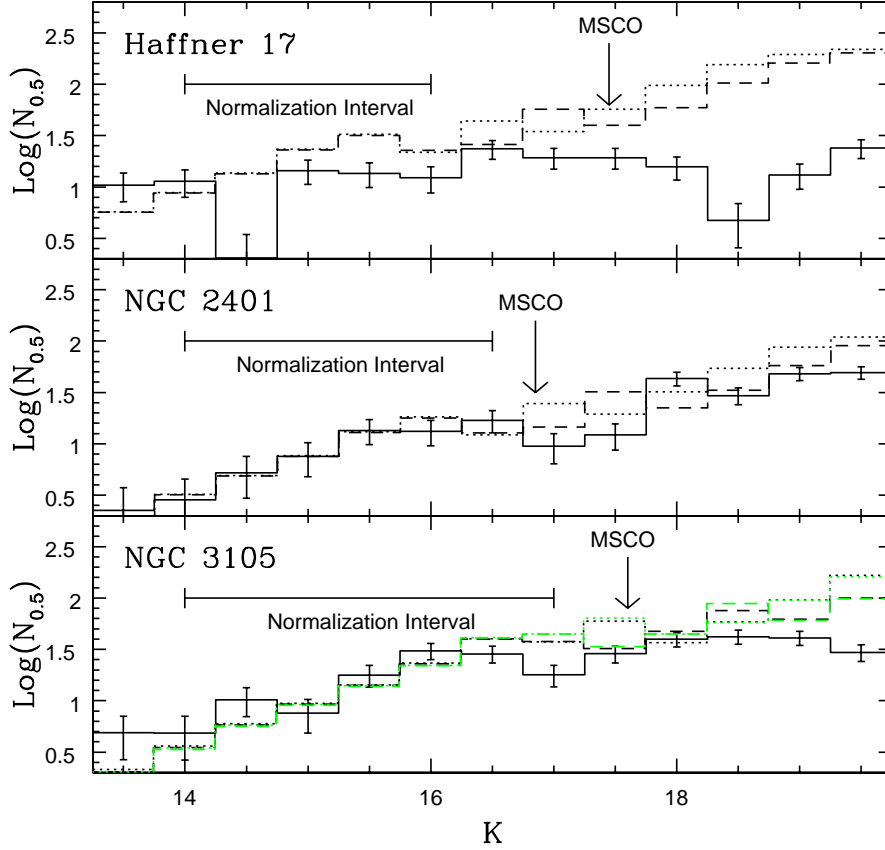


Fig. 7.—  $K$  LFs.  $N_{0.5}$  is the number of objects per 0.5 magnitude interval in  $K$ , corrected for field stars. **The artificial star experiments indicate that the number counts in all three clusters are complete for  $K < 19.5$**  The mean of the upper and lower limits of the MSCO is indicated for each cluster. Model LFs with  $Z = 0.016$  and ages  $\log(t) = 7.4$  (dotted line) and  $7.6$  (dashed line) are also shown. The distance moduli and reddenings obtained in Section 4 are used for these comparisons, and the models have been scaled to match the observed LFs in the magnitude intervals indicated. There is reasonable agreement between the models and the observations of NGC 2401 over most magnitudes. However, this is not the case for the other clusters. The models do not match the Haffner 17 LF when  $K \leq 15$  and  $K \geq 17$ . As for NGC 3105, the models reproduce the slope of the LF when  $K \leq 16$ , but tend to fall above the observed LF at fainter magnitudes. The green lines in the bottom panel show the result of adopting a distance modulus for NGC 3105 that is 0.15 dex closer than that found from the  $Z = 0.016$  sequences, and there is little difference when compared with the models that use the larger distance modulus.



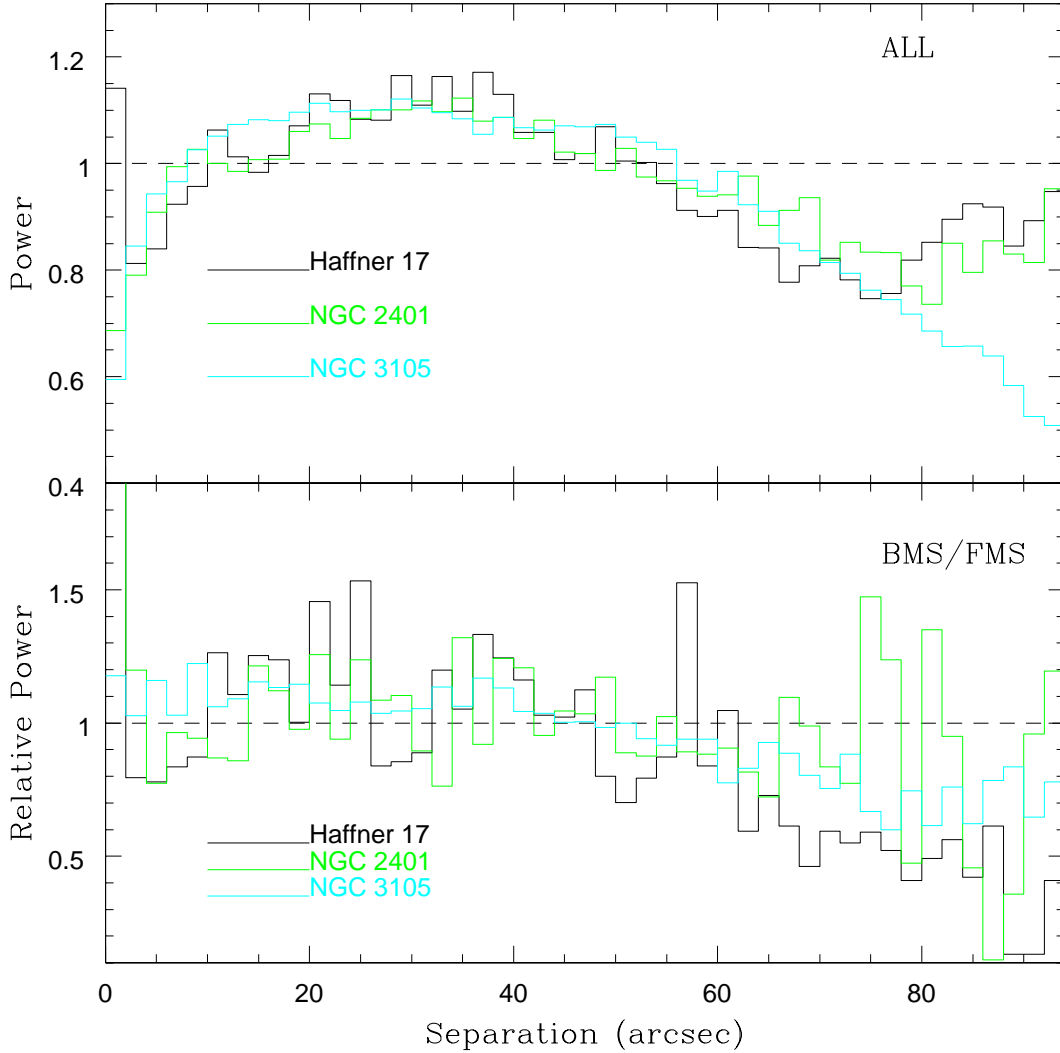


Fig. 8.— TPCFs. The bin-to-bin jitter at intermediate separations provides a rough estimate of the statistical noise in these curves (e.g. Davidge 2012). The TPCFs of the ALL samples are similar for separations  $< 80$  arcsec, except in the bin that samples the smallest separation. The peak in the Haffner 17 TPCF at the smallest separations suggests that this cluster may have a larger population of wide binaries than NGC 2401 and NGC 3105. The ratio of the BMS and FMS SFs, shown in the bottom panel, is close to unity for most separations in NGC 2401, indicating that the BMS and FMS samples have similar clustering properties. However, the ratio of the SFs of Haffner 17 and NGC 3105 dips below unity at separations  $> 60$  arcsec, indicating that the objects in the BMS sample are more centrally concentrated than those in the FMS sample. In Figure 9 it is demonstrated that field star contamination likely affects the TPCF of both clusters at large separations, although not enough to erase the differences in the BMS and FMS distributions.

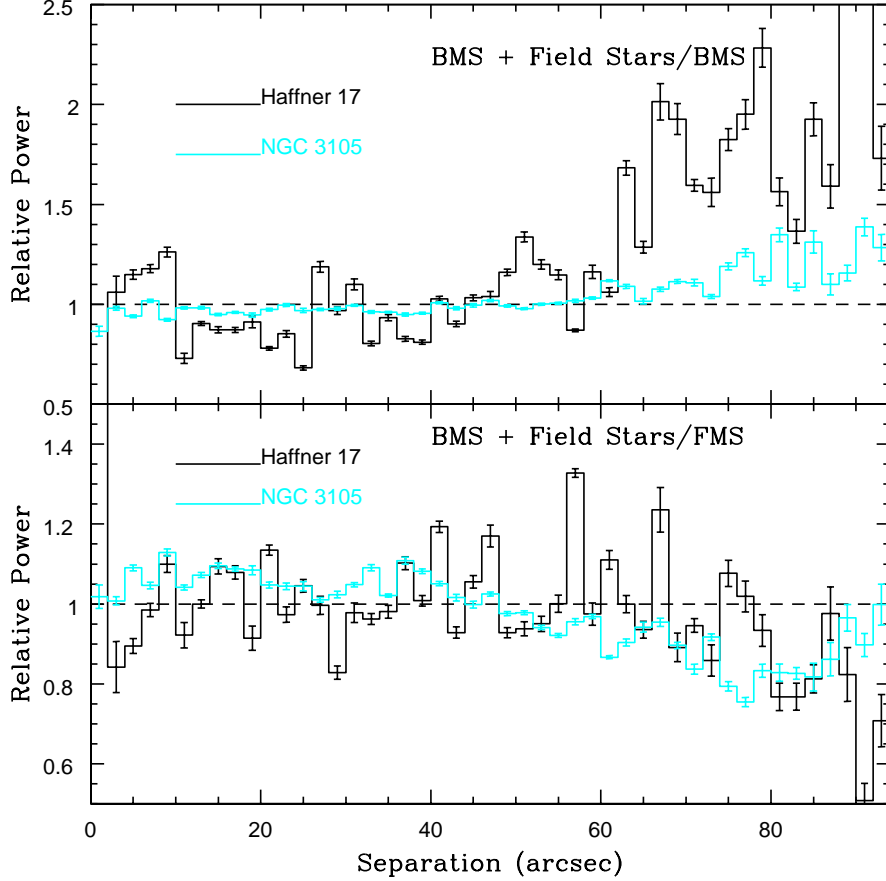


Fig. 9.— Field star contamination and clustering. The top panel shows the ratio of the SFs of the BMS + artificial field star samples and the measured BMS SFs. The BMS+field star SF is the average of a number of realizations, and the error bars show the dispersion about the mean at each separation. Adding a population of uniformly distributed objects has a marked impact on the BMS TPCFs of both clusters at separations  $> 60$  arcsec. The bottom panel shows the ratio of the BMS + field star sample and FMS TPCFs. Balancing differences in field star contamination causes the TPCF ratio for Haffner 17 to become flatter than in Figure 8, although at separations  $> 80$  arcsec the TPCF still falls consistently below unity. The objects in the FMS sample of NGC 3105 are also more uniformly distributed at large separations after adding field stars than those in the BMS sample. The members of the BMS and FMS samples that belong to Haffner 17 and NGC 3105 appear to have different clustering properties, in the sense that the fainter members are more uniformly distributed than the brighter, more massive members.